Available online at www.sciencedirect.com
ScienceDirect
Journal of Power Sources 173 (2007) 325–345
JOURNAL OF POWER SOURCES
www.elsevier.com/locate/jpowsour

Thin films for micro solid oxide fuel cells

D. Beckel *, A. Bieberle-Hütter, A. Harvey, A. Infortuna, U.P. Muecke, M. Prestat, J.L.M. Rupp, L.J. Gauckler

Nonmetallic Inorganic Materials, Department of Materials, ETH Zürich, Wolfgang-Pauli-Str. 10, CH-8093 Zürich, Switzerland

Received 13 February 2007; accepted 29 April 2007
Available online 5 May 2007

Abstract

Thin film deposition as applied to micro solid oxide fuel cell (μSOFC) fabrication is an emerging and highly active field of research that is attracting greater attention. This paper reviews thin film (thickness ≤1 μm) deposition techniques and components relevant to SOFCs including current research on nanocrystalline thin film electrolyte and thin-film-based model electrodes. Calculations showing the geometric limits of μSOFCs and first results towards fabrication of μSOFCs are also discussed.

Keywords: Thin film; Micro solid oxide fuel cell; Cathode; Anode; Electrolyte

1. Introduction

Solid oxide fuel cells (SOFCs) convert chemical energy with high efficiency directly into electricity and heat and can operate on a variety of fuels such as natural gas or hydrogen. As depicted in Fig. 1, the fuel supplying H_2 is fed into the anode compartment where it is oxidized, and the electrons released as a result are conducted to an external circuit [1]. The reaction products on the anode side of an SOFC are mainly water and CO_2. Air enters on the cathode side and oxygen is reduced here to O^{2-} by reaction with electrons from the external circuit. The O^{2-} ions can travel through the ion-conducting and gas-tight electrolyte, which separates the anode compartment from the cathode compartment. Once on the anode side the O^{2-} joins with hydrogen to form water. The driving force for an SOFC is the difference in oxygen partial pressure between the anode (low pO_2) and cathode (high pO_2). Open circuit voltage (OCV) is the voltage obtained at zero current that ranges from about 0.8–1.1 V and is a measure for the gas leakage or electronic leakage through the electrolyte. A low OCV reduces the SOFC power output.

The choice of materials for each component is given by the requirements resulting from the functions discussed above: The anode must be porous to allow gas access, should be a catalyst for fuel oxidation and must show electronic and ionic conductivity. Nickel satisfies the first two requirements, while yttria-stabilized zircona (YSZ) or cerium gadolinium oxide (CGO) fulfills the last. Therefore, two-phase cermets (ceramic-metal composites) that combine all three properties are used. The electrolyte should be dense and predominantly an ionic conductor like YSZ or CGO while the cathode should be porous to enhance gas access, catalytically active towards oxygen reduction, and a good ionic and electronic (mixed) conductor. For cathodes perovskites are commonly chosen, for example $La_xSr_{1-x}MnO_{3\pm\delta}$ (LSM), $La_xSr_{1-x}Co_yFe_{1-y}O_{3\pm\delta}$ (LSCF) or $Ba_{0.5}Sr_{0.5}Co_{0.8}Fe_{0.2}O_{3\pm\delta}$ (BSCF) [2] or precious metals such as Pt [3].

Differing from this two-gas-chamber concept is the single-chamber SOFC [4], where the anode and cathode are exposed to the same gas atmosphere, a mixture of fuel and air in a safe ratio. Here the driving force is the locally different oxygen partial pressure at the electrodes, which is generated by the different selectivity of the anode and cathode towards fuel oxidation [5–7]. For a recent review see [8].

Typical operating temperatures for current thick-film-based two-chamber SOFCs are 800–1000 °C, placing heavy demands on the materials and complicating the sealing mechanism. Therefore, research trends towards lowering the operating temperature down to 500–600 °C. To compensate for the performance losses associated with a lower operating temperature, thin film components with lower ohmic resistance have been developed. Thin film components facilitate the fabrication of μSOFCs, leading to

* Corresponding author. Tel.: +41 44 632 3763; fax: +41 44 632 1132.
E-mail address: Daniel.Beckel@mat.ethz.ch (D. Beckel).

0378-7753/$ – see front matter © 2007 Elsevier B.V. All rights reserved.
doi:10.1016/j.jpowsour.2007.04.070

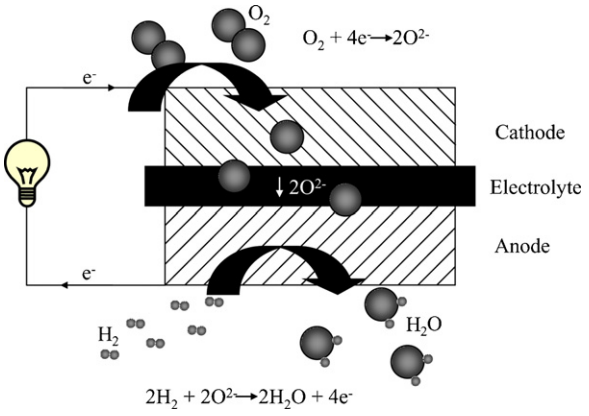

Fig. 1. Sketch of an SOFC illustrating also the working principle.

new applications for SOFCs, namely portable electronic devices such as laptops, personal digital assistants (PDAs) and scanners [9,10].

The scope of this review primarily encompasses the emergent fields of thin film deposition for SOFC components, μSOFC fabrication with thin films, and the properties of the thin film materials themselves.

2. Thin film deposition techniques

The choice of an appropriate thin film deposition technique is strongly influenced by the material to be deposited and the desired film quality and available budget. This section gives an overview of the most relevant thin film deposition techniques for SOFC applications as well as some examples of SOFC materials where these techniques were used for deposition.

2.1. Vacuum deposition techniques

For thin film growth in vacuum deposition, gas-phase atoms of the chosen material are transported from the source to the substrate, upon which the film will nucleate and grow. The whole process takes places in a vacuum chamber, where the atmosphere and gas-phase reactions can be controlled carefully (for the basics of vacuum technology the reader is referred to e.g. [11]). Strict control of the residual gases in the environment becomes more important as the deposition rate is lowered and the influence of contaminants on the film properties is raised. A recent review of the application of vacuum techniques to SOFC materials in general can be found in [12,13]; the current review is limited to thin films only.

2.1.1. Physical vapor deposition (PVD) techniques

PVD techniques have the common feature that atoms are brought to the gas phase through a physical process from a solid or molten target. The processes include: evaporation, sputtering, laser ablation and hybrid methods. Chemical reactions in the gas phase and at the substrate are absent, or at least irrelevant. However, simple oxides and nitrides can be grown from metallic substrates by introducing oxygen or nitrogen gas during processing. The most prevalent of these techniques for SOFC materials is sputtering, but pulsed laser deposition (PLD) is becoming more and more popular. Evaporation of complex materials, which many SOFC components are, is difficult and scarcely used. PLD and sputtering are both expensive techniques from the point of view of equipment, and have similarly low deposition rates of a few nm per minute. The films are typically polycrystalline with columnar structure, and the grain size can be tailored by varying the deposition conditions, and nano-sized grains are easily obtained.

Thin films deposited by PVD methods can be porous or dense depending on the process parameters, temperature having the highest impact on the structure as described in the structure zone models of PVD film growth [14,15]. Films deposited in low adatom (short for "adsorbed atom" and describing associations of a few atoms) mobility conditions show a structure of columns and voids at the nanoscale, with sizes increasing with the film thickness even though not linearly.

2.1.1.1. Sputtering. In the sputtering process (apparatus shown in Fig. 2A) material is removed from a solid cathode target by bombardment with positively charged ions emitted from a noble gas discharge. The high kinetic energy ions colliding with the surface break free, or sputter, atoms of the cathode in a process of momentum transfer. In the case of DC sputtering, a high negative voltage (3–5 kV) is applied to the target from a source external

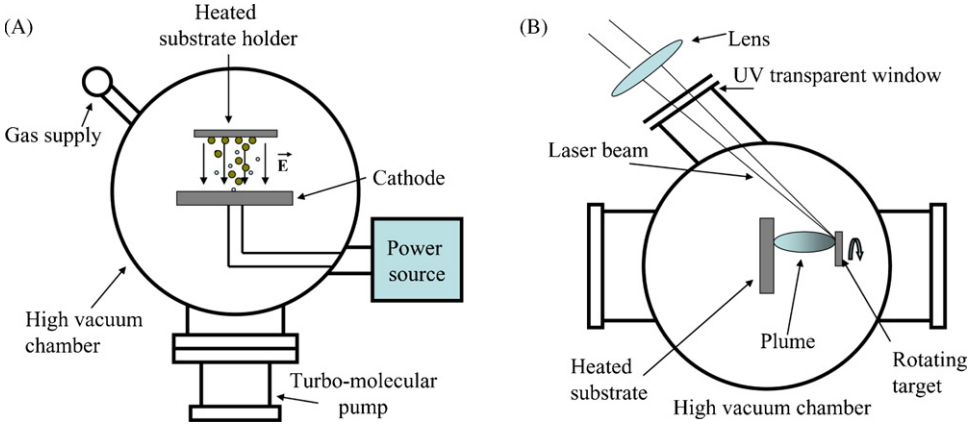

Fig. 2. (A) Schematic representation of a generic sputtering system. (B) Schematic representation of a generic PLD deposition system.

to the vacuum chamber; while the chamber and the substrate are grounded. A noble gas (commonly Ar) introduced between the target and substrate is subjected to an electric field high enough to induce ionization and generate a plasma of positive ions and electrons. The positive ions are accelerated toward the negatively charged target and sputtering results. With metallic targets the potential at the cathode is provided by a DC source, but a radio frequency (RF) source is needed for sputtering dielectric materials.

Higher sputtering efficiency and deposition rates are obtained with magnetron sources, which use a magnetic field to confine the electrons in the plasma close to the target where they can regenerate the plasma and increase its density. Numerous reviews on sputtering are available [16–19], but the focus of this review is on applications for SOFC fabrication. Sputter deposition, both DC and RF, was employed prior to PLD for thin film deposition in the SOFC field.

All three elements of a fuel cell – anode, electrolyte and cathode – have been studied and realized in thin film form. Previous publications refer to single-layer studies or cases where one of the elements, often the anode or the electrolyte, serves as support for the whole system with one or both of the other two elements in thin film form. Predominantly, thin film electrolytes have been prepared, particularly YSZ [20,21] and CGO [22,23]. However, porous Ni/YSZ anodes [24] on dense YSZ substrates as well as anodes and electrolytes on porous substrates such as alumina [25] have been successfully grown as thin films. The deposition of the cathode material lanthanum strontium cobaltite (LSC) was also reported [26]. Deposition is usually performed at low temperature (<400 °C) in a partial pressure of oxygen in the order of 10 mTorr. Post-deposition thermal treatment in air is then necessary for crystallization and densification of the electrolytes. Even the deposition of an entire SOFC was reported [27] but the electrolyte (YSZ) was rather thick (15–20 μm) and not fully dense.

2.1.1.2. Pulsed laser deposition (PLD). PLD is a physical method of thin film deposition in which a pulsed laser beam, usually of wavelength in the UV range, is employed to ablate a target composed of the desired thin film material, which is subsequently deposited onto a substrate. PLD has attracted much attention over the last 20 years, as it enables fabrication of multi-component stoichiometric films from a single target. The experimental PLD setup (Fig. 2B) consists of a vacuum chamber containing target and substrate holders; the chamber is equipped with a UV-transparent window through which the laser beam enters the chamber. Outside the chamber, a UV-transparent lens focuses the laser beam onto the target surface. The use of additional optical elements, such as mirrors and beam splitters, depends on the system complexity. Because each element reduces the intensity of the beam, the optical path has to be designed carefully. The evaporation power source, i.e. the laser, is decoupled from the vacuum system making the technique very flexible.

The useful range of laser wavelengths for thin film growth by PLD lies between 200 nm and 400 nm for most materials. With an appropriate choice of the laser, any material can be ablated and the growth can be carried out in a pressure of any kind of gas, reactive or not.

The laser-target interaction is a very complex physical phenomenon, which depends on the laser characteristics and the optical, topological and thermodynamic properties of the target. Upon absorption by a solid surface, the electromagnetic energy of the laser beam is converted first to electronic excitation and then to thermal, chemical and mechanical energy causing evaporation. From the point of view of film formation, the important fact is that ablation takes place in a time interval short enough to suppress the dissipation of energy beyond the ablated volume. In this way, the damage of the remaining target can be minimized and segregation of the different components largely avoided.

Targets, usually disk shaped, are normally rotated and moved with respect to the laser beam in order to suppress surface roughening. Mostly ceramic targets are used. Dense small-grained targets are preferable because single-crystalline or coarse-grained polycrystalline ones are damaged by thermal shock after a few pulses and particle ejection becomes more likely. Dense ceramics absorb the radiation better and have lower thermal conductivity thanks to their grain boundaries. Both properties enhance the local material–radiation interaction. The ablated species consist of energetic evaporants (atoms, molecules, electrons, ions, clusters) with energies ranging from 10 eV to over 100 eV depending on the material, congruent with the target. Together they constitute what is called the plume. After irradiation, the plume rapidly expands in a jet that remains narrow and relatively anisotropic, allowing for deposition of small areas only. The most important obstacle for the application of PLD in industrial production is the difficulty in scaling-up the process. However, possible evolutions of PLD that would allow for large-scale deposition have been proposed [28,29].

Reviews detailing the mechanisms and some applications of PLD can be found elsewhere [30,31], with this review restricted to thin films deposited by PLD for SOFCs to which the technique has been applied recently. Porous and dense perovskite electrodes [32–34], electrolytes such as CGO [35–37], YSZ [38], lanthanum strontium gallium manganite (LSGM) [39–41] and samaria doped ceria (SDC)/LSGM bilayer [42] have all been deposited by PLD. An entire thin-film-based SOFC was produced by PLD [43] comprising a YSZ electrolyte and LSC cathode both on top of a micro-structured Ni grid that served as an anode (see also Section 4, this work). Amorphous dense films with or nano-size grains can be obtained in low oxygen partial pressure (<10 mTorr) at low temperature and then crystallized by annealing in air. In the cases of CGO and YSZ, it was found that the porosity and the presence of cracks were strongly influenced by the deposition pressure [44] and higher density was obtained at lower pressure.

2.1.2. Chemical vapor deposition (CVD)

The techniques described above use some physical process to remove atoms or molecules from a target. In the case of CVD (Fig. 3A), a reactive gas transports precursors of the desired material to the substrate. Here, they react with other gases or decompose to give the final product deposited on the substrate in the form of a film. The carrier gas flows through the different

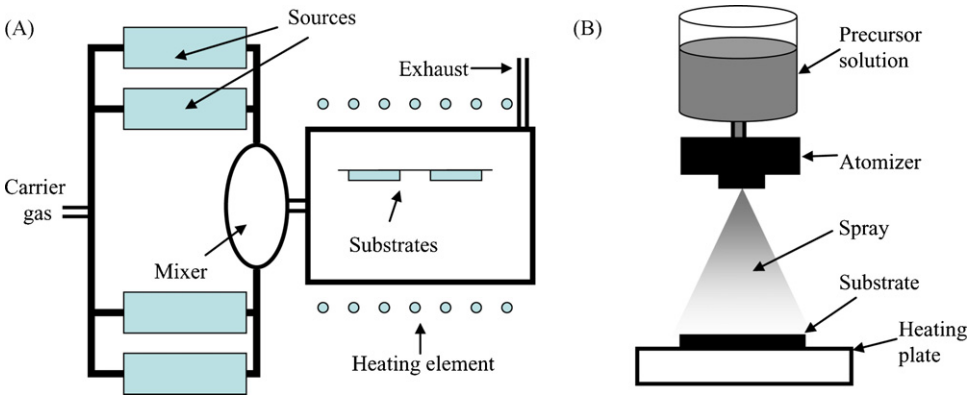

Fig. 3. (A) Schematic representation of a generic CVD reactor. (B) Schematic representationof a generic spray process.

source materials and carries some along. Precursor materials are mixed in the carrier gas flow before being introduced in the reaction chamber, where the reactive mixture flows across the substrate and a set of reactions takes place under the energy provided by heaters or by a plasma discharge (Plasma Enhanced CVD, PECVD).

CVD does not require the use of high vacuum but processing in a low-pressure environment enables the production of high quality and high purity films not achievable with conventional CVD. Widely employed in the semiconductor industry, CVD is used for SOFC fabrication with low pressures. Many different deposition methods have been derived from CVD with the purpose of increasing the deposition rate, enhancing the reaction efficiency or simply to develop a low-cost deposition method [45].

For an extensive review on the basics of the CVD process as well as some application examples, the reader is referred to [46] and for a very recent review to [47]; this review is restricted to examples of fuel cell materials deposited by CVD.

CVD processes have been mainly used to produce dense, gas-tight, electrolyte films, 1–10 μm thick, on dense and porous substrates [13,48]. Because the pores of the substrate can be easily closed by this process, CVD is particularly convenient when the electrolyte has to be grown on a porous anode substrate. However, porous cathodes were also realized [49]. One example of a variation of CVD is atomic layer deposition (ALD), a technique that allows the production of dense films less than 1 μm thick by building one mono-atomic layer after another [50]. This method was used to grow thin electrolyte layers [51,52]. Another example is electrochemical vapor deposition, where film growth proceeds because of an electrochemical potential gradient existing between the two sides of the substrate [13].

2.2. Liquid-precursor-based thin film deposition techniques

Wet-chemical processes are used extensively to produce coatings and thin films for fuel cells, protective coatings or microelectronic devices. The different techniques used to apply the solutions to the substrate can be divided into brush painting, the most basic method, spraying, dipping and spinning.

2.2.1. Spray deposition methods

There is a broad choice for the nomenclature of spray deposition techniques; sometimes categories overlap and authors use different terminologies. All methods involve the generation of a fine aerosol of a liquid precursor solution, which is then directed towards a heated substrate surface with or without the aid of an external electric field as depicted in Fig. 3B. Depending on the substrate temperature and precursor used, the droplets evaporate or decompose completely before reaching the substrate, resulting in a process resembling to CVD [53], or the liquid is deposited without evaporation. Burning a flammable precursor might be used to form a particulate spray or reach higher deposition temperatures. The different spray techniques are mainly distinguished by the method of atomization, which can be accomplished by means of pressurized gas or application of a high electric field to the solution surface at the spray nozzle. Using standard photolithographic lift-off processes or shadow masks, films can be deposited on flat surfaces in patterns.

In ceramics processing, spray pyrolysis was originally used for the production of nanometer-sized powders and the synthesis of different materials was extensively studied [54]. Lately it has been replaced by high-volume, low-cost flame spray pyrolysis processes [55]. Interest in spray pyrolysis was renewed when the need for thin film electrolytes in high-temperature fuel cells arose. This publication highlights the few papers that deal with thin film production for SOFC applications, for example electrolyte and electrode materials. For a detailed overview of thin film materials produced by spray pyrolysis the reader is referred to the paper by Patil [56]. The annex of the work of Pamplin [57], originally dealing with the preparation of solar cell materials by spray pyrolysis, contains a bibliography of references on the method up to the year 1979. Tomar and Garcia [58] reviewed the production of thin films for solar cells and oxide semiconductor films for gas sensors. The production and properties of nanocrystalline materials and coatings are detailed in [59]. An overview of technical aspects of the spray setup and description of the deposition of solar cell materials are given by Mooney and Radding [60]. Albin and Risbud [61] describe the spray processing and influential parameters of optoelectronics materials. A part of the review by Chopra et al. [62] on transparent conducting films is devoted to spray pyrolysis processing. In another

paper [63] the authors give a detailed overview of the physical and chemical processes involved in spraying. Will et al. [13] dedicate a part of their review paper on thin solid electrolytes to the spray pyrolysis method. Bohac and Gauckler [64] give a description of various techniques for the chemical spray deposition of ceramic films. The most up-to-date review on thin film deposition using spray pyrolysis with emphasis on SOFC electrolyte materials was recently published by Perednis and Gauckler [65]. De Jonghe et al. [66] give a description of supported electrolyte thin film synthesis.

2.2.1.1. Electrostatic spray deposition (ESD). ESD involves applying a high potential to the surface of a conducting liquid or precursor, which, under the forces of the electric field, generates an almost mono-sized spray from the charged repulsion between droplets. Very porous and regular structures were produced by Schoonman and coworkers [67] which sparked interest in this technique amongst the fuel cell community. Porous electrode films of LSCF [68,69], LSM [70], LSM/YSZ [71] and dense electrolyte films of YSZ [72–75] and CGO and LSGM [76] have been produced.

2.2.1.2. Flame spray deposition. Flame or combustion spray synthesis is a method for one-step synthesis and deposition of porous or dense ceramic layers onto heat resistant surfaces. The process can be either a mainly physical process when a suspension of fine oxide particles in a flammable liquid carrier is utilized, or physical and chemical when metal salts in a flammable solvent mixture are used as educts for the ceramic coating formation. On burning in the combustion flame, collision and sintering of the particles in the flame occurs and a coating is formed on the substrate placed in or near the tip of the flame. CGO and samarium strontium cobaltite (SSC) [77], YSZ [78,79], pure cerium oxide [80] and LSM [81] have been produced by this technique.

2.2.1.3. Pressurized gas spray deposition (PSD). In PSD, atomization of the precursor is achieved by a pressurized carrier gas, e.g. air. Setoguchi et al. [82] were among the first to utilize the PSD technique for thin film production related to SOFCs. They fabricated a calcia-doped zirconia thin film from acetylacetonates in ethanol on a porous LSM substrate. Due to the low deposition temperature of 80–200 °C the film was cracked and multiple depositions were necessary to obtain a nearly dense film. Later, Bohac and Gauckler [83] revisited the process and permutated various solvents and salts to form YSZ and CGO films. Perednis et al. published the successful deposition of dense YSZ films with thicknesses <500 nm and porous buffer layers of yttria doped ceria (YDC) [84,85]. Physical characteristics of the setup used, for example droplet size distributions and droplet velocities, are given in [75]. Cells fabricated with these films reached power densities in excess of 750 mW cm^{-2} at 770 °C [86]. The same group is working on the fabrication of layers less than 500 nm thick of dense CGO [36,37,87,88], porous LSCF [89–91] and porous Ni-CGO cermets [92,93] for μSOFC.

Putna et al. [94] utilized the PSD method to deposit SDC thin films on CGO substrates, but almost no experimental details were disclosed. Charpentier et al. [95–97] produced thin films of LSM on Ni-YSZ anode substrates. A combined approach of spray pyrolysis and sol–gel methods was chosen by Vo et al. [98] to produce cells with mixed gas atmosphere.

2.2.1.4. Ultrasonic spray pyrolysis (USP). Randomly and preferentially oriented YSZ films were prepared by Matsuzaki et al. [99] with ultrasonic spray pyrolysis. The liquid precursor was ultrasonically nebulized and a carrier gas stream was used to transport the fine mist towards the substrate. Films based on lanthanum chromite [100] and ceria layers [101] have also been produced with USP.

2.2.1.5. Mist spray pyrolysis (MSP). MSP is not strictly a liquid-precursor-based deposition technique, but involves spraying a liquid precursor into a furnace where very fine oxide particles are formed by oxidation of the metal salts. The particles are then deposited directly from the air stream on the substrate material and sintered to form dense films. Priestnall and Steele [102] have deposited lanthanum strontium copper oxide as possible electrode material, but the material was not used further and the process, being too cumbersome, was abandoned.

2.2.2. Electrophoretic deposition (EPD)

EPD is a simple and fast deposition technique to produce thin films from colloidal particles. Powder particles are charged and suspended in a colloidal system. Under the forces of an externally applied electric field, the particles move to the substrate surface and coagulate in a dense layer. Peng et al. [103] utilized EPD to deposit dense YSZ layers on porous LSM cathode substrates, others [104,105] deposited YSZ on NiO-YSZ anode substrates.

2.2.3. Spin- and dip-coating

The spin- and dip-coating processes are widely utilized to produce thin ceramic coatings on a variety of substrate materials. Thin film deposition with spin-coating consists of applying a precursor solution on one side of a rapidly rotating substrate whereas during the dip-coating process the substrate is partly or fully immersed in the precursor solution with both sides and then withdrawn from the liquid. A huge variety of precursors may be used for these techniques.

2.2.3.1. Metal organic decomposition (MOD). In this technique, the precursor is a chemical solution containing metal salts and one or more organic species. The organic compounds evaporate partly during or after deposition and the resulting film pyrolyzes upon annealing to form a ceramic coating with the desired stoichiometry. Metal carboxylates are often used as metal salts and dissolved in a suitable solvent. Chu et al. [106] demonstrated the deposition of pure zirconia, yttria and YSZ films from neopentanoates. Hayashi et al. [107] produced LSM/YSZ composite film electrodes by the MOD technique. The solution used was a mixture of octylates of La, Sr and Mn in a solution of iso-propanol containing triethanolamine and butoxides of Zr and Y in a solution of iso-propanol and diethanolamine.

LSC [108] and lanthanum manganite films doped with Ca, Sr or Ba [109] were synthesized in much the same way as above with a solution based on neodecanoates in xylene.

2.2.3.2. Polymeric precursors/sol–gel method. The sol–gel process is based on liquid-phase hydrolysis of organo-metallic salts like metal alkoxides to form a colloidal sol and a condensation step with organic monomers to form a gel. The particle concentration, viscosity, concentration and stability of the sol–gel influence the deposition parameters and film quality and have to be controlled carefully. Numerous reviews concerning the sol–gel method have been published. Brinker et al. [110] studied the fundamentals of sol–gel dip-coating and the physics of sol–gel thin film formation by dip-coating [111]. Dunn et al. [112] give a brief overview on sol–gel approaches for solid electrolyte and electrode materials. The sol–gel section of this review will elaborate on fuel cell related materials, e.g. YSZ or CGO rather than including all possible sol–gel methods reported in the literature so far.

Some groups [113,114] distinguish between polymeric precursor and sol–gels. Polymeric precursors are produced by combining metal or metalloid cations with weak organic acids and a polyhydroxyl alcohol as a chelating agent and monomer. These form a very stable precursor solution after polymerization of the alcohols that is insensitive to air and ageing over a prolonged period of time. Unlike sol–gels, fabrication of polymeric precursors does not include a distinct gelation step. Polymeric precursors involve the evaporation of water from a highly viscous solution, which often leads to boiling retardation. However, others [115] refer to polymeric precursors as sol–gels. In this review no distinction is made between polymeric precursor and sol–gel techniques. The distinction is in the chemistry of the precursors.

Alkoxide precursors: Kim et al. [116–118] studied the zirconium *n*-butoxide, yttrium nitrate, acetic acid, nitric acid, water and iso-propanol system to obtain a spinnable precursor gel, whereas Mehta et al. [119] prepared thin YSZ films on yttria-doped ceria substrates from a gel containing zirconium and yttrium iso-propoxide, nitric acid, iso-propanol and water. Kueper et al. studied a sol–gel deposition of YSZ on porous LSM with zirconium *n*-propoxide and yttrium iso-propoxide, methanol and iso-propanol as solvents and diethanolamine as network modifier. A similar approach with the same salts but ethyl acetoacetate as chelating agent was followed by Peshev and Slavova [120]. Changrong et al. [121] obtained gels using zirconium *n*-propoxide and yttrium nitrate.

Sol–gel or polymeric precursors have mainly found interest in the production of electrolyte thin films. Only a limited number of studies are available on the production of thin film electrode materials, as opposed to the large number of publications available on the production of electrode powders from sol–gels. Hwang et al. [122] obtained porous lanthanum cobaltite films with a gel produced with lanthanum iso-propoxide, cobalt acetate, 2-ethylacetoacetate, 2-methoxyethanol, polyethyleneglycol and water. The same authors also studied the fabrication of lanthanum manganese oxide [123] and Sr-doped lanthanum cobaltite thin films [124].

The shelf-life of sol–gel alkoxide precursors is relatively short and the chemicals used are moisture sensitive, so the wet chemistry has to be performed under a protective gas environment, making the process costly and difficult to control.

Halogenide precursors: Gorman et al. [125] and Dong et al. [126] utilized zirconium oxychloride and yttrium nitrate as starting salts for the preparation of a spin-coating solution with water, tartaric acid and ethylene glycol to form YSZ thin films. Chen et al. [127] used the same salts and replaced the tartaric acid by glycine to produce YSZ thin films. A chloride-based polymeric precursor was used by Brezesinski et al. [128] to obtain mesoporous ceria, zirconia and ceria-zirconia structures with pore sizes of about 10 nm and grain sizes of 5–7 nm.

It should be noted that with salts containing halogenides it is possible for some amount to remain in the film, leading to unwanted side effects such as different densification properties or changes in conductivity [114].

Nitrate and acetate precursors: Anderson and coworkers [114] investigated a spin-coating process to fabricate YSZ and SDC films [113] based on an alkoxide- and halogenide-free polymeric precursor solution. Lenormand et al. [115] and Wang et al. [129] also produced thin films of lanthanum ferromanganite and LSM, respectively, without using alkoxides or halogenides. Gaudon et al. detail the cost-effective production of an LSM [130] and LSM-YSZ [131] composite via a solution-polymerization process similar to the Pechini [132] process.

Layer-by-layer deposition: Moriguchi et al. [133–137] developed a two-dimensional sol–gel process as novel method to deposit sub-nanometer ultra-thin titania and zirconia films. A gel film is formed on a water surface and deposited on a substrate layer-by-layer. The organics are removed by heating and simultaneously initiating the gel-oxide transition.

2.2.3.3. Impregnation. Difficulties in applying a film with thickness more than 1 μm and limitations to dense substrates have stimulated the development of a combinatorial process, called “net-shape” technology [138,139] to produce YSZ films. A colloidal suspension is first applied onto the substrate to form a porous film, which is then followed by the impregnation with a polymeric precursor solution. Others have used gels [140] or aqueous solutions [141] for impregnating porous YSZ or modifying existing cathodes with LSM or CGO coatings.

2.2.3.4. Slurry-coating. Dip-coating or spraying [142,143] with ceramic particulate or colloidal suspensions (“slurry-coating”) is only mentioned briefly here, as the thickness of the films produced is generally larger than a few microns and limited sometimes to the particle diameter in the dipping solution which is usually a few hundred nanometers [144–149]. Advances towards finer particulate suspensions for YSZ electrolyte layers have been reported [150,151].

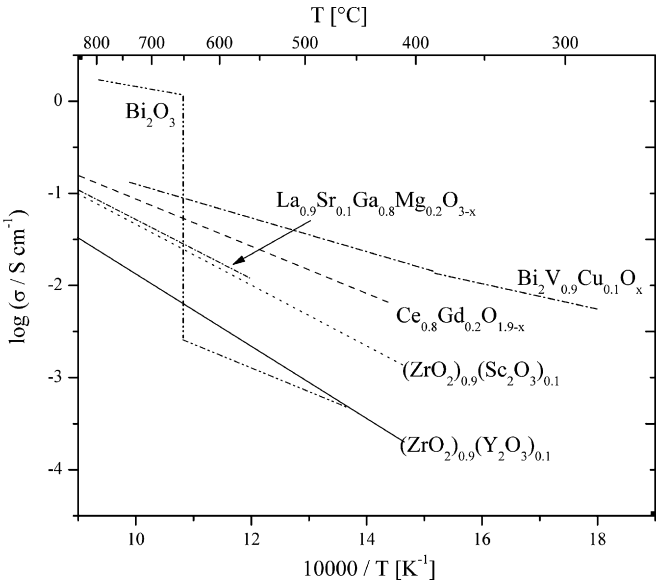

Fig. 4. Ionic conductivity of different microcrystalline electrolyte materials [167–169].

3. Cell components

In this section, the current work on thin film components (anode, electrolyte and cathode) for SOFCs is reviewed.

3.1. Electrolytes

Today's state-of-the-art electrolytes are usually 10–200 μm thick and are mainly produced by powder processing or by thick film techniques, such as tape-casting. In order to decrease SOFC operating temperatures from 800 °C to 1000 °C to about 500 °C and to reduce the costs of the system, thin film methods are favorable. Main advantages of using thin films are: (i) the decreased film thickness, being 100 to 1000 nm, lowers the ohmic losses across the fuel cell, (ii) the processing allows sintering temperatures below 1000 °C or even no sintering at all and (iii) the possibility exists to manipulate the electrical conductivity by controlling the nanocrystalline microstructure of a thin film. It was found that nanocrystalline materials show, in most cases, unusual electrical conductivities [152–157] and thermal stabilities [36,158–162] because of their high amount of grain boundaries with respect to grain area. In the case of nanocrystalline thin films, stresses within the film that result from the thermal expansion mismatch between the substrate and the thin film or from the deposition process can affect the electrical conduction properties and have to be considered [163].

In this review, microstructure and electrical conductivity characteristics of SOFC thin film electrolyte materials are summarized. A comparison of the electrical conductivity of the nanocrystalline SOFC thin film electrolytes (Tables 1 and 2), to microcrystalline electrolytes [164–166] is given in Fig. 4 [167–169].

Among the microcrystalline electrolyte materials YSZ is used most often. YSZ is a predominantly ionic conductor for temperatures up to 1000 °C and thus good for SOFC use. However,

Table 1
Comparison of YSZ thin films electrical and microstructure properties

Chemistry	Technique	Microstructure				Electrical conductivity		Ref.
		Film thickness (nm)	Charac-teristics	Substrate (nm)	Average grain size (nm)	Activation energy of total conductivity (eV)	Total conductivity at 700 °C (S m^{-1})	
$(ZrO_2)_{0.98}(Y_2O_3)_{0.03}$	CVD	500–2000	Dense	Al_2O_3 (102)	50–200	1.1	–	[178]
				MgO (100)		1.3		
				SiO_2		0.9		
$(ZrO_2)_{0.95}(Y_2O_3)_{0.05}$	CVD	340	Dense	Si (111)	80–100	1.08	0.157	[257]
		500–2000	Dense, columnar	Al_2O_3 (102)	50–200	1.3	–	[177]
				MgO (100)		1.1		
				SiO_2		0.9		
$(ZrO_2)_{0.92}(Y_2O_3)_{0.08}$	PSD	100–500	Dense	Sapphire	9.8	1.19	0.37	[65]
$(ZrO_2)_{0.91}(Y_2O_3)_{0.09}$	PVD	100–1000	Dense	Si_3N_4	5–10	grain: 1, grain boundary: 0.69	–	[21]
$(ZrO_2)_{0.90}(Y_2O_3)_{0.10}$	PLD	>2000	Dense, epitaxial	MgO	–	1.09	1.58	[258]
$(ZrO_2)_{0.84}(Y_2O_3)_{0.16}$	Spin coating	100–600	Dense	MgO	–	1.1	3.64	[127]
	PLD	<2000	Dense	Polycrystalline Al_2O_3	20	0.93	–	[259]

Table 2
Comparison of $Ce_{0.8}Gd_{0.2}O_{1.9-x}$ thin films electrical and microstructure properties

Technique	Microstructure					Electrical conductivity		Ref.
	Film thickness (nm)	Characteristics	Substrate (nm)	Average grain size (nm)	Microstrain (%)	Activation energy of total conductivity (eV)	Total conductivity at 700 °C (S m^{-1})	
PVD	400	Dense	Polycrystalline Al_2O_3	110	–	0.95–1.05	0.251	[260]
			Quartz				7.94	
Spin coating	110–630	Dense	Sapphire	9	1.5	1	0.630	[185]
				15	0.2	1.2	0.319	
				36	0.02	1.3	0.039	
PLD	1000	Dense, epitaxial	$NdGaO_3$	–	–	2.5	0.74	[261]
	200–800	Dense	Sapphire	46	–	0.81	2.139	[180]
				55		0.88	1.783	
				75		1.01	0.754	
PSD	200–400	Dense	Sapphire	18	2.09	0.68	–	[180]
				29	0.89	0.76	2.010	
				59	0.32	0.93	3.193	
				76	–	1.04	0.909	

Fig. 4 shows that YSZ exhibits lower electrical conductivity compared to alternative microcrystalline electrolytes such as scandia-stabilized zirconia (SSZ), CGO, LSGM or bismuth vanadium copper oxide (BIMEVOX) [170,171]. Among the highly conductive electrolytes, CGO has become more and more popular [172,173], as long-term degradation and phase stability problems during SOFC operation are still unsolved problems for YSZ, SSZ, LSGM and BIMEVOX materials. In contrast to YSZ, CGO is a so-called "mixed ionic-electronic conductor" with ionic and electronic conductivity at low oxygen partial pressures and temperatures higher than 800 °C [174–176]. It is, therefore, mainly used for intermediate- to low-temperature SOFC operation where ionic conductivity prevails.

The best investigated thin film electrolytes so far are YSZ and CGO. With respect to thin film quality, it is found for both materials that sputtering, PLD and CVD can result in columnar thin films (see Fig. 5A) that may even grow epitaxially on a substrate, whereas spin coating and PSD usually result in non-columnar microstructures, as shown in Fig. 5.

3.1.1. Yttria stabilized zirconia (YSZ)

Table 1 summarizes the electrical and microstructural properties of YSZ thin films with 3–16 mol% Y_2O_3 doping of the zirconia lattice, produced by various thin film deposition methods. For comparable doping concentrations, YSZ thin films show high deviations in the activation energies and electrical conductivity even though the same thin film technique was chosen. In general, the activation energy of electrical conductivity varies between 0.9 eV and 1.3 eV for YSZ thin films depending on the level of doping and the microstructure.

In studies of $(ZrO_2)_{0.95}(Y_2O_3)_{0.05}$ deposited by CVD onto different substrates with a constant film thickness and a constant average grain size [177,178], a severe impact of the substrate material on the electrical properties was found. The authors proposed that the mismatch of thermal expansion coefficients (TEC) between the substrate and the YSZ resulted in differently compressed thin films states, affecting the electrical conductivity. The lowest activation energy of 0.9 eV was measured for the case where the compressive stress in the thin film was the largest, and the highest activation energy of 1.3 eV was measured for the thin film with the lowest compressive stress. The idea that the amount of strain present in a thin film affects the electrical properties is currently under discussion [163,179–181]. It is assumed that thin films composed of a host crystal lattice doped to a high degree with a dopant of different valency and ionic radii – as it is the case for CGO or YSZ – have a high amount of chemical stress which affects the electrical conductivity. It was found that YSZ thin films [86] show 3.5 times lower ionic

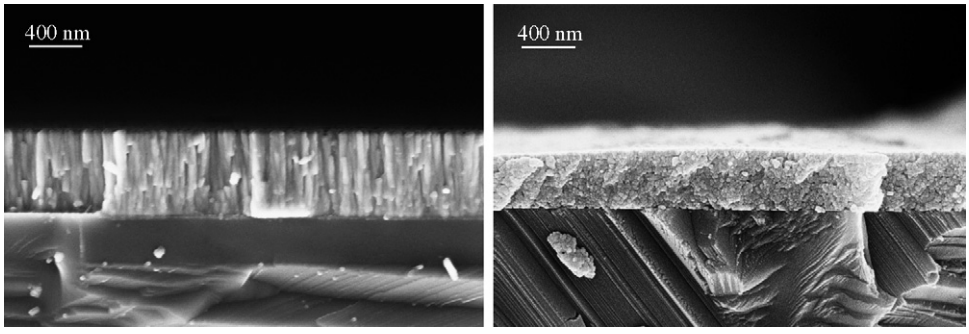

Fig. 5. Cross-section micrographs of (A) CGO deposited by PLD showing columnar microstructure and (B) CGO deposited by PSD with isotropic microstructure.

conductivity than microcrystalline samples [65]. However, for SOFC operation the lower conductivity is more than compensated for by a lower ohmic resistance of the 10–100 times thinner electrolyte. Indeed, Perednis and Gauckler [86] obtained more than 600 mW cm^{-2} at 700 °C with 500 nm thick bi- and trilayer electrolytes of YSZ and YDC deposited by PSD. Nevertheless, for electrolyte thicknesses in the range of the electrode particle size resistance decreases less than linearly with thickness [182]; therefore excessive thinning of the electrolyte has a low impact on the electrolyte resistance (see also Section 4.1 of this work).

3.1.2. Ceria gadolinia oxide (CGO)

Table 2 shows for CGO thin films deposited by PLD, spin-coating and PSD that decreased microstrain results in an increased activation energy and lower total conductivity. It was observed that the total conductivity of CGO at 700 °C varies mostly between 0.75 S m^{-1} (low microstrain) and 3.18 S m^{-1} (high microstrain) (Table 2) and remains 5–1.25 times smaller than the ionic conductivity of microcrystalline CGO [174,183,184]. In the case of PSD fabrication of CGO thin films [180], the activation energy of ionic conductivity increased from 0.68 eV to 0.93 eV for a microstrain decrease of 2.09% to 0.32%, and for a spin-coated film [185], the activation energy increased from 1 eV to 1.3 eV for a microstrain decrease from 1.5% to 0.02%. In those experiments, different levels of microstrain in the thin films were achieved by different annealing temperatures, whereby the microstrain decreased during crystallization (and grain growth) with increasing annealing temperature. Different thin film preparation methods and different substrates lead to different initial stresses and the corresponding microstrain within the CGO (or YSZ) thin films will be different as well.

CGO thin film electrolytes deposited by PSD were also used to improve the gas tightness of traditional thick film SOFCs and to prevent interface reactions, such as the formation of insulating La-zirconate at the interface between YSZ electrolytes and LSM cathodes. It was shown that vacuum-plasma sprayed SOFCs have a better power output by more than 20% if a CGO film of roughly 200 nm thickness is deposited between the LSM cathode and the YSZ electrolyte [186].

Besides the geometric constrains for electrolytes discussed above (Section 3.1.1) other considerations are also important for CGO electrolytes. Due to its mixed ionic electronic conductivity the electrolyte thickness has to be chosen carefully. If the electrolyte is too thin, the electronic conductivity will prevail and depress the cell performance. A detailed study on this issue can be found in [187].

3.1.3. Lanthanum strontium gallium manganite (LSGM)

Up to now only little research has been done on thin film electrolytes alternative to YSZ or CGO. Taniguchi et al. [76] and Mathews et al. [188] reported on the deposition of LSGM thin film electrolytes by ESD and PLD, respectively. In the case of sprayed LSGM [76], so far it has not been possible to produce dense thin films that would achieve the requirements of a thin film SOFC electrolyte. In addition, no electrical conductivity or detailed microstructural investigations have been made on LSGM thin films.

3.1.4. Bismuth oxide-based electrolytes

In the field of Bi_2O_3-based electrolytes, δ-Bi_2O_3 thin films have recently been produced by CVD [189–191]. The authors reported that δ-Bi_2O_3 thin films remain stable even down to temperatures of 350 °C. The highly conductive δ-Bi_2O_3 changes usually to phases with lower symmetry and low conductivity between 730 °C and 650 °C for microcrystalline Bi_2O_3-based ceramics (Fig. 4) and are, therefore, not feasible as an SOFC electrolyte [192,193]. However, if a phase stabilization of δ-Bi_2O_3 down to 350 °C is possible in thin films, electrical conductivity characteristics and long-term phase stability investigations would be of high interest.

3.2. Anodes

Anode thin films can be applied in μSOFCs or used for the investigation of electrode reaction mechanisms. State-of-the-art anodes have a very complex microstructure including three interpenetrating networks of Ni, YSZ (or CGO), and a gas phase, (e.g. a porous Ni-YSZ [CGO] cermet). Also, the anodic reaction mechanism consists of a large number of steps that are difficult to separate. Hence, model electrodes made of thin films having a well-defined geometry have been investigated by several groups using experiments or simulation as a simpler system to elucidate anode reactions. Besides these thin film electrodes, Ni-point [194–197] and Ni-paste [198] electrodes were studied but these approaches suffered from non-reproducibility, contacting and scaling issues. In the following sections, we will discuss in some detail the experimental and simulative studies on model thin film anodes.

3.2.1. Structured Ni thin films

From the experimental side, first studies on model anodes using well-defined structures were published several years ago by Mizusaki et al. [199], de Boer [200], and Bieberle et al. [201]. All three groups focused on metallic Ni thin films microstructured to a line pattern by photolithography and wet chemical etching. Feature sizes down to 5 μm were realized. The triple phase boundary lengths (l_{tpb}) were increased by almost three orders of magnitude [201]. A light microscope image of a Ni pattern with equidistant lines of 20 μm, resulting in a total tpb length for a 1 cm^2 sample of 3.7 m cm^{-2}, is shown in Fig. 6. The thin film patterns were stable up to temperatures of about 700 °C. Higher temperatures result in substantial grain growth and coarsening of the Ni [199]. The electrochemical performance of the anodes as measured by electrochemical impedance spectroscopy was very similar in [201] and [200], while much lower electrode conductivities were reported by [199]. In all studies, one main rate-limiting step and a linear relationship between the electrode conductivity and the tpb length were found, signifying that the reaction proceeds through the tpb. However, considerable disagreement exists in the identification of the rate-determining reaction step. While Mizusaki et al. [199] claimed that the rate-limiting process is either dissociative adsorption of reactants

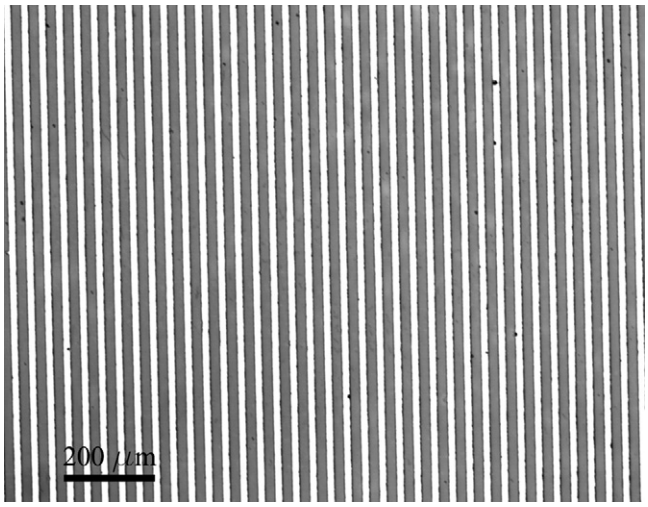

Fig. 6. Light micrograph of a Ni pattern anode on single crystalline YSZ; equidistant lines of 20 μm width and an ideal tpb length of 3.7 m cm^{-2}.

or surface diffusion of adsorbed species on the Ni surface, de Boer [200] suggested that a reaction limited by a charge transfer process with YSZ has an active role in the electrode kinetics. Bieberle et al. [201] attributed the main impedance arc either to adsorption-desorption of hydrogen or to the removal of O^{2-} from the electrolyte, while both processes might be combined with a charge transfer process. An increase in the partial pressure of water in the fuel gas was found to have a catalytic effect on the anode kinetics and a mechanism with hydroxylated YSZ surface was suggested [201].

Despite these detailed and very similar experimental studies on thin film Ni patterned anodes, the reaction mechanism even in this very simplified system is not fully understood and no general consensus exists about the rate-limiting reaction step. However, it is generally accepted that these model experiments give very detailed insight into the kinetics. This explains why the approach with thin film model Ni electrodes has re-emerged recently. Sukeshini and Habibzadeh [202] prepared Ni patterned anodes and studied the electrochemistry with dry and wet fuels, such as H_2, CO, CH_4. First preliminary results predicted a mechanism dependent on the Ni surface area, which is in contradiction to the previously mentioned studies. However, higher operating temperatures of 750–900 °C and different YSZ surface conditions might be responsible for the disagreement. It was found that adsorption–desorption equilibration may play a decisive role in the oxidation of both CH_4 and CO. Ehn and Hogh [203] found for Ni line patterned anodes similar reaction rates for H_2–H_2O and CO–CO_2. However, the electrode reactions seemed to be affected by impurities at the tpb. Both groups have announced more detailed studies for the future, in particular with respect to carbonaceous fuels.

3.2.2. Simulations

In parallel to the experimental studies, simulations are carried out in order to investigate the reaction mechanism. Simulations based on model electrode geometries allow direct comparison with experimental data and thus allow for the estimation of kinetic data that are not readily available for these systems (high temperature and ambient pressure) from the literature. Since experimental data is rare and kinetic parameters are unknown, all simulation studies are very preliminary so far. A good overview on the kinetics of the Ni, H_2–H_2O | YSZ system is given in [204]. Here, kinetic parameters were estimated with the help of literature and first simulation results on this system were published. Starting from an electrochemical model, the kinetics were transformed into a state-space model which allowed the determination of surface coverages of adsorbed species as well as rate constants by numerical simulation with experimental data from Ni patterned anodes [201]. This study showed for the first time that the Ni anode system can be simulated directly from an electrochemical model with good agreement to experimental data of Ni patterned anodes. The same experimental data, the same electrochemical model and kinetic data, and a very similar simulation approach were used by Bessler [205]. The better agreement between experimental and simulated impedance spectra in this study and the better consistency to the literature cannot be attributed to the few differences in the simulation approach, i.e. simulation in the time domain and maintenance of the nonlinear response, but is most probably related to a more elaborate fitting and simulation procedure. Additional features in the simulation approach of Bessler not in [204] were the simulation of the transient behavior and of the gas-phase diffusion within a stagnation layer above the electrode but both these elements could not unambiguously explain the reaction mechanism up to now. However, more detailed simulations are planned for the future, which will also discuss in detail the influence of the water on the reaction mechanism. In [206], Bessler et al. simulated for the first time Ni-YSZ cermet anodes from an electrochemical model. The disagreement compared to experimental data showed that the electrochemical model used was only an incomplete description of the real processes taking place at a cermet anode. Detailed studies on the gas-phase transport were published in [207]. It is stressed that the so-called gas concentration impedance consists of contributions from the bulk gas phase, from diffusion, and from convection. All these contributions are closely coupled and cannot be separated in their impedance response.

Additional simulations on line-pattern anodes were recently published by Goodwin [208]. The simulations were based on an electrochemical model similar to the simulations by Bieberle and Gauckler [204] and Bessler [206] also using hydrogen as fuel. However, here, the formation of hydroxyl from hydrogen and water was not included in the model. The simulations were compared to the experimental data of Mizusaki et al. [199], de Boer [200], and Bieberle et al. [201]. The results showed that the electrochemical model could reproduce much of the observed electrochemical response from the experiments on thin film patterned anodes. More detailed and more complex simulations using hydrocarbon fuels are foreseen for the future.

Finally, Williford and Chick [209] simulated the effects of surface diffusion on concentration polarization by means of Pt model electrodes. They claimed that the common assumption that the reactions are confined to the tpb is very questionable and

that a tpb width of several hundred Angstroms on polycrystalline Pt is a more realistic picture.

3.2.3. Porous anode thin films

Literature on porous thin film anodes is scarce. Porous Ni/YSZ cermet anodes have been fabricated by sputtering [24,27,210] and porous Ni CGO anodes by PSD [92,93]. These anodes are intended for use in thin-film-based μSOFCs rather than to study reaction mechanisms, as is done with the model electrodes.

3.3. Cathodes

Similar to anodes, most work on thin film cathodes has been devoted to model cathodes to study the mechanisms involved in the cathode reaction.

3.3.1. Oxygen reduction

Oxygen reduction at SOFC cathodes follows a sophisticated reaction path that has been drawing much attention [211]. Today's cathodes are viewed preferably for intermediate and low operating temperatures (<600 °C). They are often made of mixed ionic–electronic conducting perovskites (ABO_3) where both the A sites (a rare earth element, such as lanthanum) and the B sites (a transition metal) can be substituted in order to tailor the material properties. Compositions with lanthanum partially substituted by strontium ($La_xSr_{1-x}BO_{3\pm\delta}$) have been extensively used ([167] and references therein). In those compounds, the Sr^{2+} cations sit on the La^{3+} sites because of similar ionic radii. The substitution of La^{3+} by Sr^{2+} creates a fully ionized acceptor level (Sr'_{La}) whose charge is compensated by holes ($B^{\bullet}_{B}$) in the valence band as well as oxygen vacancies ($V^{\bullet\bullet}_{O}$). $La_xSr_{1-x}BO_{3\pm\delta}$ perovskites are therefore highly doped p-type semiconductors [212–214]. Typical materials are the well-known LSM, LSCF and BSCF [2]. Oxygen can be transported through the bulk of the perovskite by a hopping mechanism via the oxygen vacancies. The concentrations of the defects in the perovskite structure are dependant on the chemical composition, the temperature and the oxygen partial pressure.

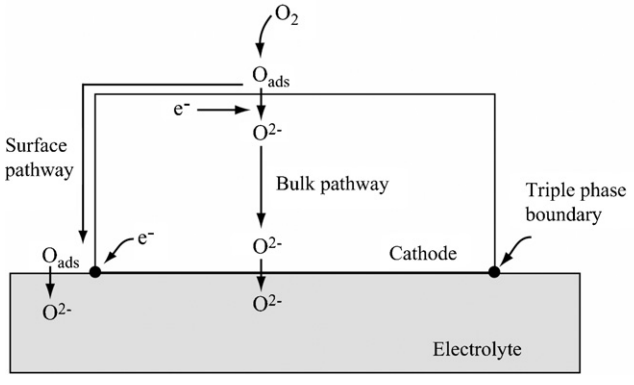

Fig. 7. Schematic representation of the possible oxygen reduction pathways for a mixed ionic–electronic cathode. Bulk and surface pathways are parallel, i.e. in competition.

Fig. 7 schematically describes the possible reaction pathways of oxygen reduction. Bulk and surface pathways are parallel, i.e. in competition. The fastest path determines the overall kinetics of the reaction. One pathway may be dominant or both may have similar importance, depending on the rate constants of the reaction steps. The nature of the rate-determining pathway determines the optimal microstructure of the cathode. The mechanism of oxygen reduction involves many reaction steps, such as adsorption; dissociation; gas-phase, surface and bulk diffusion; and charge transfer. When the bulk pathway plays a significant role, the defect chemistry of the electrode has to be taken into account as well. Modeling oxygen reduction is therefore an arduous task whereby many parameters have to be handled. The need to simplify the investigated systems and gain a better understanding of oxygen reduction has stimulated the development of thin, dense geometrically well-defined (gwd) films over porous electrodes. The complex description of gas-phase diffusion through the electrode pores can be disregarded. Most important, key-parameters such as the tpb length and bulk diffusion length (i.e. film thickness) can be controlled.

3.3.2. Geometrically well-defined cathodes

Several studies have been published on gwd cathode thin films. Few are devoted to fabrication and processing-related issues, and instead focus on the investigation of the reaction mechanism.

3.3.2.1. Studies of the reaction mechanism. The oxygen reduction pathway at thin $La_{0.9}Sr_{0.1}MnO_{3-\delta}$ electrodes has been visualized by Horita et al. [215–217]. After deposition on YSZ with RF sputtering, the film of 490 nm thickness was microstructured as a mesh with photolithography and atomic etching techniques. Oxygen reduction was performed at and out of equilibrium using the stable $^{18}O_2$ isotope as a marker. The samples were quenched and analyzed with secondary ion mass spectroscopy (SIMS) at various points of the electrode, notably at the LSM surface and close to the LSM/YSZ interface. This qualitative approach to oxygen reduction showed that thin LSM films promote the bulk pathway especially at high overpotentials.

Brichzin et al. [218] used gwd, dense circular $(La_{0.8}Sr_{0.2})_{0.92}MnO_{3-\delta}$ microelectrodes and measured their impedance as a function of the diameter. The films were prepared by PLD followed by microstructuring with photolithography and etching. The resulting electrodes had a thickness of 100 nm and a diameter, d, ranging between 10 μm and 200 μm. The polarization resistance was found to be dependant on d^{-2}. In a continuing work a linear dependence between the electrode thickness and the polarization resistance was established [219]. The authors concluded that the bulk pathway is dominant, in contrast to the common view that LSM, whose oxygen transport properties are known to be poor [220], favors the surface pathway. Similarly, Baumann et al. [221] investigated the impedance of thin microstructured $La_{0.6}Sr_{0.4}Co_{0.8}Fe_{0.2}O_{3-\delta}$ electrodes and concluded the same as Brichzin with regard to the preferred reaction bulk pathway.

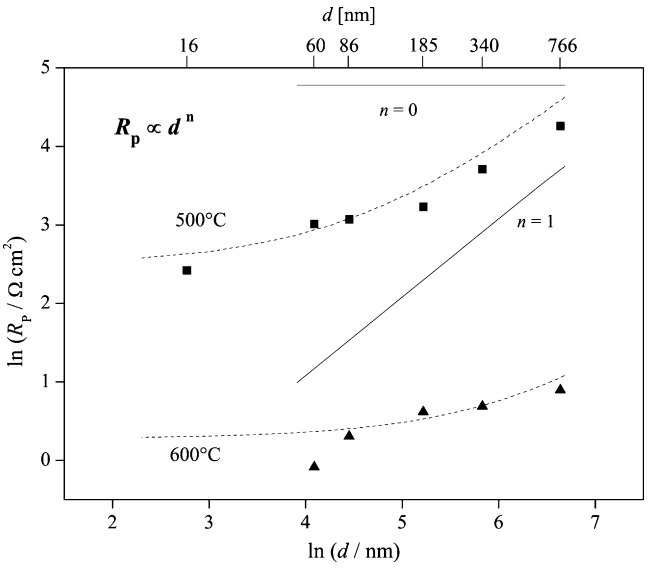

Fig. 8. Polarization resistance R_p of oxygen reduction at thin dense $La_{0.52}Sr_{0.48}Co_{0.18}Fe_{0.82}O_{3-\delta}$ electrode as a function of the thickness d at 500 °C and 600 °C at equilibrium [34,224,225]. The full symbols (■, ▲) represent the experimental data. The dashed lines represent the simulated data from the model obtained after numerical optimization. Oxygen bulk diffusion is evidenced to be one of the rds of the reaction.

Koep et al. [222] investigated oxygen reduction using arrays of $La_{0.8}Sr_{0.2}MnO_3$ stripe electrodes. The LSM patterns with 260 nm thickness were prepared using RF sputtering and photolithographic techniques. To determine the contribution of the bulk pathway, the oxygen reduction impedance of the LSM electrodes was measured with and without a thin insulating TiO_2 layer on top. The role of the TiO_2 was to block the oxygen access to the LSM–gas interface while leaving the triple phase boundary active. The significantly larger polarization resistance obtained for the TiO_2-covered electrode confirmed the findings of Brichzin [218,219], i.e. a contribution of the bulk pathway and a large area specific resistance (ASR).

The use of gwd electrodes allows to study the influence of geometry on the kinetics, both from the experimental and theoretical point of view [223]. Prestat et al. investigated oxygen reduction at thin dense gwd $La_{0.52}Sr_{0.48}Co_{0.18}Fe_{0.82}O_{3-\delta}$ electrodes by combining state-space modeling of the Faradaic impedance and experimental measurements [34,224,225]. The thickness of the square-shaped films was varied between 16 nm and 800 nm while the surface area remained unchanged (3 mm × 3 mm). Simulations showed the contribution of the surface pathways is negligible for electrodes with such geometry. Bulk diffusion of oxygen vacancies was determined to be one of the rate-determining steps by the increase of the polarization resistance upon increasing the film thickness (Fig. 8). The other rate-limiting step (adsorption and incorporation) were identified using a numerical optimization between modeling and experimental data. Rate constants of the rate-determining step were assessed and found to depend on the thickness of the cathode. Besides these physical models that aim for understanding of the reaction mechanism, other theoretical work is based on providing equivalent circuits to simulate the behavior of a mixed conducting electrode [226].

3.3.2.2. Fabrication related studies. Most related to fabrication is the work by Bieberle-Hütter and Tuller [26]. They investigated the microstructuring of LSC into interdigitated electrodes on different substrates. It was found that the etching quality was strongly dependent on the substrate material (decreasing quality from Si to CGO to YSZ) meaning that even at a temperature of less than 500 °C, LSC interacts with the substrate and forms some interface. Hence, for feature sizes of less than 50 μm, a microfabrication process alternative to etching has to be used. The electrical and electrochemical characterization of the interdigitated LSC electrodes showed a strong influence of the thin film deposition parameters on the conductivity [227]. The substrate selection was found to be important not only with respect to fabrication of the pattern [26] but also with respect to electrical disturbance. Detailed electrochemical analysis of the LSC electrodes was not possible due to the geometrical constraints.

3.3.3. Cathode performance: thin films versus porous thick films

Though thin films were first considered as model systems to investigate the fundamentals of oxygen reduction, they can also be utilized to increase the performance of SOFC cathodes. This is notably true for miniaturized systems where traditional ceramic techniques (like screen-printing) cannot be applied for practical reasons. Discrepancies about the performance of thin cathode films still exist in the literature. Sirman et al. [228] compared the impedance of porous and dense $La_{0.6}Sr_{0.4}Co_{0.2}Fe_{0.8}O_{3-\delta}$ electrodes. The dense electrode with 1 μm thickness showed a significantly larger polarization resistance than the porous one. Those findings contradict the results reported by Steele and Bae [229] for the same perovskite. In this work, the authors measured the influence of a dense LSCF layer (∼1 μm thick) placed between a porous LSCF film and CGO electrolyte. The area specific resistance of the electrode with the dense film was 2–3 times lower. More recently, Prestat et al. compared the current-potential plots of porous LSCF electrodes with and without an LSCF thin dense film adjoining the electrolyte [34,224]. The performance was improved when the film was sufficiently thin (<ca. 60 nm) and poorer when the dense layer was too thick (>ca. 340 nm). This suggests that high performance could be achieved by coating the electrolyte with an ultra-thin cathode film (see Fig. 9). The loss of the tpb (contribution of the surface pathway) would be compensated for by a complete coverage of the electrolyte by the active material. The kinetic losses due to bulk diffusion would be reduced significantly by minimizing the film thickness as much as possible. Materials with facile charge transfer at the electrode–electrolyte interface and with fast incorporation of oxygen should be sought. Promising advances in this field have been recently reported in the literature [2]. Moreover a recent paper of Baumann et al. [230] suggests that electrochemical performance could be "activated" by applying a large voltage bias to thin film cathodes. In the case of $La_{0.6}Sr_{0.4}Co_{0.8}Fe_{0.2}O_{3-\delta}$, the effect is attributed to the change of cation stoichiometry close to the surface. However,

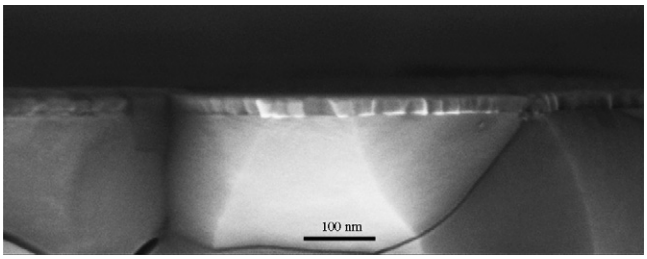

Fig. 9. Cross-section micrograph of an ultrathin dense $La_{0.52}Sr_{0.48}Co_{0.18}Fe_{0.82}O_{3-\delta}$ layer prepared by PLD. The substrate is a polished cerium-gadolinium oxide pellet.

at the time of writing, this type of electrochemical activation had not been proven to be stable with time.

3.3.4. New issues raised by thin films

Besides the beneficial aspects from the investigations of reaction mechanisms and kinetics, employing thin films also presents some drawbacks and establishes new relevant questions.

3.3.4.1. Geometric considerations. Reaction kinetics depend not only intrinsically on the nature of the material but also on the electrode geometry. Thus, one has to keep in mind that the data obtained on thin layers (in the sub-micrometer range) with large surface area cannot be directly transposed to porous electrodes with a typical grain size of ca. 1 μm. For instance, the thin LSM electrodes of Brichzin et al. [218,219] exhibit a specific resistivity of ca. 400 Ω cm^2 for LSM at 800 °C, which is much greater than other data reported in literature [231]. This can be attributed to the fact that the geometry of the electrodes (the diameter was much greater than the thickness) forced the reaction to occur through the bulk of the LSM, which does not transport oxygen ions efficiently.

3.3.4.2. Current collection. Current collection is another crucial issue. When working with thick porous electrodes (typically > 10 μm) prepared by conventional ceramic processing methods, such as screen-printing, this task is relatively straightforward. A metallic gauze (made of platinum, for instance) is pressed on the layer in its green state. Co-firing the paste and the current collector yields a good "intimacy" and reliable mechanical stability between the components. Homogeneous potential distribution is achieved throughout the bulk of high conductivity materials like LSCF and LSM. Current collection is more arduous when dealing with thin electrodes. Besides the fact that the films do not have any green state, two contradictory requirements have to be fulfilled: On one hand, molecular oxygen should have access to the film, which implies a sufficiently open porosity. On the other hand, in order to ensure a homogeneous potential distribution when working out of equilibrium, the current collector should fully cover the thin layer in the ideal case. Different approaches to meet these constraints have been reported in the literature, each of them having its own advantages and drawbacks.

Brichzin et al. [218,219], Baumann et al. [221,230] and Yildiz et al. [223] collected the current by means of a tungsten carbide tip when using LSM and LSCF microelectrodes, enabling a homogeneous access of oxygen to the ga–electrode interface. The contribution of the tip to the oxygen reduction can be neglected. Yet, when working with thin films, this kind of point contact may lead to heterogeneous potential and current distribution within the electrode. This may explain the huge area specific resistivity of LSCF reported by Baumann [221] (10 Ω cm^2 at 750 °C), i.e. around two orders of magnitudes greater than that of porous electrodes [232].

A thin dense silver layer may also be employed since oxygen can be transported through it and a homogeneous potential distribution at the electrode–current collector interface is ensured. Conversely, it does not enable one to investigate the adsorption and incorporation of oxygen at the perovskite–gas interface. Application as such of a silver layer could be suitable for studies focusing particularly on the bulk properties of the electrode, such as diffusion coefficient. Ringuede and Fouletier [233] utilized this kind of current collector to investigate oxygen reduction of $La_{0.7}Sr_{0.3}CoO_{3-\delta}$ electrodes.

Platinum is a standard current collector in SOFC experiments. Several authors utilized it as paste or gauze to contact thin cathode films [228,234,235]. Although this kind of current collector is rather straightforward to set up, it may also significantly affect the kinetics of the thin film–gas interface. In theory, the incorporation of oxygen in the perovskite electrode is chemical in nature and involves no charge transfer. The oxygen is incorporated on oxygen vacancies and holes are created within the perovskite. That means no charged species crosses the gas-perovskite interface. The charge transfer occurs at the perovskite-electrolyte interface, where the oxygen vacancies (and the O^{2-} ions, respectively) cross the interface. By introducing a metallic current collector that is active towards oxygen reduction, it is then no longer clear whether oxygen is reduced directly by the perovskite or by the platinum. In other words, oxygen reduction can occur at the platinum–perovskite–gas interface as well. Hence the experimental kinetic data, such as adsorption and incorporation rate constants, cannot be unambiguously assigned to the investigated thin film only.

Prestat et al. used a porous LSCF film as current collector to investigate oxygen reduction at a thin dense LSCF film [34,224] constituting a compromise between the constraints of homogeneous potential distribution and access of molecular oxygen to the film. The porous layer was prepared by screen-printing. This approach is possible when working at macroscopic scales (in [34,224], the surface area of the electrode was 9 mm^2). The advantage is that no supplementary undesired interface is created (compared to the case of platinum current collectors described above) however, oxygen cannot uniformly adsorb on the electrode surface and it is difficult to determine to what extent the current collector may contribute to the overall kinetics of the reaction.

3.3.4.3. Defect chemistry. Another essential aspect of oxygen reduction at thin films is the defect chemistry. Solid-state electrochemistry is a peculiar type of electrochemistry, since the electro-active species (oxygen in this case) are incorporated in the bulk of the electrode and modify its composition. A

defect chemistry model is absolutely essential in the case of oxygen reduction at mixed ionic-electronic conducting perovskites. The B-site atoms are involved in the incorporation of oxygen into the mixed conductor and tied to the oxygen vacancy concentration if electro-neutrality is assumed. To the best of our knowledge, the defect chemistry of thin SOFC-related perovskite films out of electrochemical equilibrium (i.e. when a Faradaic current flows, under realistic SOFC operating conditions) has not been described yet. Facile charge transfer at the electrode–electrolyte interface and rate-limiting oxygen incorporation at the electrode–gas interface have been reported in the literature for perovskite electrodes [236]. For thin films, which "geometrically" promote the bulk pathway (large surface, thickness in the sub-micrometer range), those kinetic features favor a depletion of oxygen that may destroy the initial crystalline structure out of equilibrium. What is the maximum oxygen nonstoichiometry that the perovskite can withstand without undergoing decomposition? At high oxygen vacancy concentrations, what model can describe defect interactions? In the literature, defect chemistry models at low oxygen partial pressures involving clusters such as $\{B'_B - V_o^{\bullet\bullet} - B'_B\}^x$ [237], $\{Sr'_{La} - V_o^{\bullet\bullet}\}^\bullet$ [238,239] and, $\{B'_B - V_o^{\bullet\bullet}\}^\bullet$ [240] have been proposed for various perovskites at equilibrium. Do those models apply when an ionic current flows through the mixed conductor? Elucidating these open questions and more generally the defect chemistry of thin perovskite layers constitutes challenging and essential topics for future investigations.

3.3.5. Porous thin film cathodes

Few studies are available on porous thin film cathodes. Most studies are limited to the preparation of such layers [68,69,241,242], and only a very limited number of studies are available where typical cathode performance data such as the area specific resistance (ASR) is given [90,243]. Both publications showed that the ASR of porous thin film cathodes is not significantly different from that of porous thick film cathodes.

4. Cells

μSOFCs are currently an important issue in research [9,10], because they offer more geographical independence, higher energy densities than batteries and the possibility of fast recharging by refueling. Furthermore, the use of thin films allows lower operating temperatures. Thin film deposition is combined with micro-machining techniques in order to realize fuel cells with micron dimensions. Typically such a μSOFC would look like that depicted in Fig. 10. The gas channels are micro-machined in the supporting substrate. The thin film membrane, comprising the cell components, is deposited on the substrate. Although single-chamber SOFCs have been fabricated by micro-machining [244,245], to our knowledge there are no single-chamber SOFC based on thin films so far.

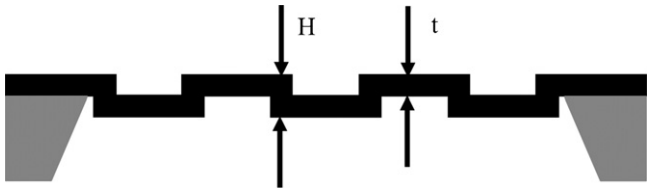

Fig. 11. Example of a corrugated membrane.

4.1. Modeling

To evaluate the feasibility of μSOFCs and to propose reasonable designs, calculations were done that took into consideration mechanical stability [246,247], electrochemical performance [182,247] as well as issues of heat losses [247].

Assuming thermal stress only and no residual stress from the fabrication processes, the stability of flat versus corrugated membranes was calculated [246]. An example of a corrugated membrane showing the geometry is shown in Fig. 11. Under compressive stress, buckling was defined as failure mode. Assuming no changes in the membrane material (YSZ in this case) with temperature, calculations showed that a corrugated membrane with a ratio of H/t = 10 can be more than one order of magnitude larger (500 μm versus 16 μm) than a flat membrane with the same thickness (1 μm) when exposed to a temperature difference between membrane and substrate of 600 °C. If tensile stress and, thus, fracture was considered as failure mode, the corrugated membrane could still take roughly twice the stress of a flat membrane. For practical use, a flat membrane with corru-

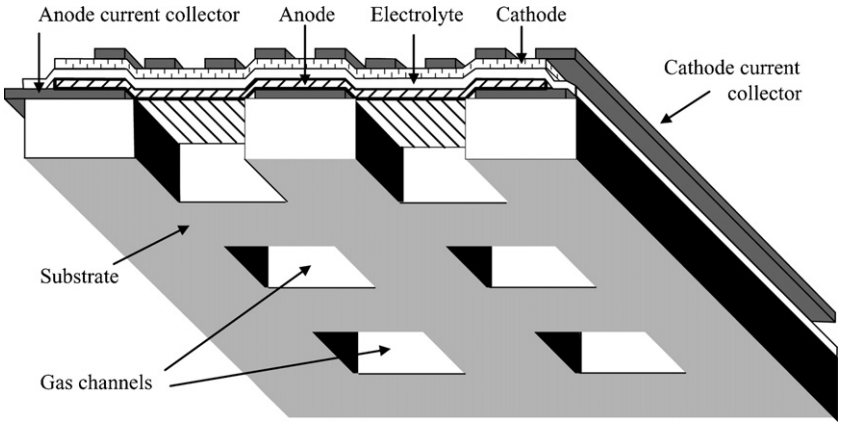

Fig. 10. Sketch of a μSOFC.

gated support on the edges might be the most useful, since the highest stress always occurs at the edge of the membrane.

In case the residual stresses of fabrication processes are known or can be tuned, they have to be added to the thermal stress [247]. In any case, from the point of mechanical stability, a thick membrane with a small radius is favorable, and a low mismatch in thermal expansion coefficient between the membrane and substrate material also improves stability. Rectangular membranes were identified to be slightly more resistant to buckling than circular or square membranes.

From the point of view maintaining a low heat loss, circular membranes were the most favorable [247], since they have the smallest perimeter for a given area. Assuming a radial temperature gradient for the membrane, with room temperature the edge of the membrane and considering heat losses through conduction only, the heat loss of the structure was calculated and found to exceed the assumed heat production of a μSOFC.

Design considerations concerning the electrochemical performance [247] were calculated using

$$P = i \times (\mathrm{OCV} - \eta_{\mathrm{Ohmic}} - \eta_{\mathrm{Activation}} - \eta_{\mathrm{Concentration}}). \quad (1)$$

With P being the power density, i the current density and η the different polarization losses. For ohmic polarization, the losses at the electrolyte were considered as follows:

$$\eta_{\mathrm{Ohmic}} = i \times \frac{t_{\mathrm{e}}}{\sigma_{\mathrm{e}}} \quad (2)$$

where t_{e} and σ_{e} are the thickness and ionic conductivity of the electrolyte, respectively. The activation polarization was calculated by

$$\eta_{\mathrm{Activation}} = \frac{R \times T}{n \times F} \times \left(\frac{i}{i_1}\right) + \frac{2 \times R \times T}{n \times F} \times \ln\left(\frac{i}{i_2}\right) \quad (3)$$

where $R = 8.314\,\mathrm{J\,mol^{-1}\,K^{-1}}$, $F = 96485\,\mathrm{C\,mol^{-1}}$, T is the temperature, n the number of electrons exchanged per oxygen ion. The exchange current densities i_1 and i_2, which are treated as free parameters, were obtained by fits to measurements from literature [248]. Concentration polarization was neglected. Based on these calculations, it was found that for an electrolyte thickness of 2 μm, the activation losses already exceed the ohmic losses by far, thus when choosing an electrolyte thickness for μSOFCs, it can be chosen with respect to mechanical stability without spoiling the electrochemical performance.

A very detailed calculation concerning the electrochemical performance of μSOFCs and single-chamber μSOFCs is given by Fleig et al. [182]. In these calculations, it was shown that the resistance of the electrolyte in a real fuel cell situation does not decrease linearly with thickness as might be expected. The reason for this behavior is the current constriction in the electrolyte. The electrodes were considered as particles sitting on the electrolyte. Depending on the reaction kinetics and conduction mechanism of the electrode material, the current is either constricted to the electrode particle–electrolyte interface, or to the tpb at the edges of the electrode particles. For both cases the electrolyte resistance decreases less than linearly with electrolyte thickness, if the electrolyte thickness is below the particle distance of the electrodes. Only by using electrodes with finer and closer packed particles a meaningful reduction in electrolyte resistance was achieved. However, the ohmic losses of electrolytes 500 nm thick at 550 °C are smaller than 0.25 Ω cm^2 for both CGO and YSZ. Thus, the performance of a μSOFC is limited by the electrodes and not by the electrolyte.

In case of single-chamber μSOFCs, geometries with interdigitated electrodes placed on one side of the electrolyte were discussed [182]. The necessary geometric constraints in order to achieve a total resistance in the cell of 1.5 Ω cm^2 were calculated. For rather thick electrodes (>1 μm), an electrode stripe width of around 10 μm would be required, while the distance between the electrodes would have to be as small as a few μm. To facilitate the micro-fabrication of such a cell, thin film technology might be considered for fabrication of the electrodes. If this were to involve a dense thin film cathode, the necessary tracer exchange coefficient of the cathode material should be $5 \times 10^{-6}\,\mathrm{cm\,s^{-1}}$ at 600 °C to match the target performance. However, this is not fulfilled by standard cathode materials, such as LSC or LSCF. On the anode side, if a thin dense Ni film would be used, further nano-structuring of the film would be needed in order to increase the tpb. These severe geometrical constraints do not only complicate the fabrication process, but the small distances between the cathode and anode may cause further problems if reaction products of the anode modify the cathode potential. The rapid transport of highly reactive products of partial oxidation ($CO + H_2$) to the cathode, as occurs for such a cell geometry, limits the performance of single-chamber SOFCs, since these products might also be catalyzed at the cathode [249].

4.2. Free-standing electrolytes

Free-standing YSZ [250,251] and CGO [250] membranes have both been fabricated on silicon substrates. For fabrication of YSZ membranes [251], SiO_2 was used as masking layer. After removing the oxide from the opposite side, YSZ was deposited by RF sputtering, and the membranes were released with wet etching. In another process, YSZ was deposited in the cavities after wet etching and the oxide was removed from the opposite side afterwards. For both processes, an annealing step at 400 °C in air was carried out after YSZ deposition in order to reduce the compressive stress in the membrane. The second process resulted in a better yield and larger membranes. Square membranes with dimensions up to 170 μm were obtained, but no tests concerning thermal stability are reported.

Baertsch et al. [250] deposited silicon nitride (SiN) on both sides of a Si wafer, which served as a masking layer for wet etching of Si on one side and as electrical insulation on the other. The electrolyte was deposited by either electron beam (e-beam) evaporation (YSZ, CGO) or RF sputtering (YSZ). Afterwards the SiN below the electrolyte was removed using dry etching techniques. The residual stress in the as-deposited thin films on the substrate was evaluated and all e-beam evaporated films showed tensile stresses around 200 MPa, independent of the film thickness, for films <1 μm. The RF sputtered YSZ films showed compressive residual stress from 850 MPa for thin (100 nm) to about 200 MPa for thick (1 μm) films. Using the same film thickness and deposi-

tion method, the yield of YSZ membranes was higher than that of CGO membranes. The maximum membrane width was roughly twice as high for YSZ (1025 μm) than for CGO (525 μm) for membranes with the same thickness. The membranes fabricated by e-beam evaporation failed during heating through membrane cracking from the center of the membrane, which was attributed to brittle fracture caused by tension. Generally YSZ membranes were able to withstand higher temperatures than CGO membranes; thicker and smaller membranes were also more robust. A high yield of more than 90% was achieved for sputtered YSZ films. Contrary to the calculated results [246,247], buckling was not considered as a failure, since buckling without fracture does not harm SOFC operation. Upon annealing at 500 °C buckling of the membranes disappeared completely and fracture via tensile stresses occurred with further annealing at 650 °C. Since the TEC of YSZ is roughly three times higher than that of the substrate material, Si, one would expect the contrary, i.e. evolution of compressive stress upon heating. Although the underlying mechanism is not fully understood, microstructural and chemical changes in the material might contribute to this result. This phenomenon also questions the use of stability calculations, where these changes in the material cannot be included easily. The work on free-standing membranes, in this case electrolytes, gives a good insight into what can be expected in terms of mechanical stability of such a ceramic thin film membrane, which is essential to know when fabricating μSOFCs.

Other studies also showed that material behaves more complex than expected. Free-standing CeO_2 membranes were fabricated by RF sputtering on Si substrates and wet etching [252]. Depending on the preparation conditions the membranes either showed buckling irrespective if the stress after deposition was tensile or compressive or, when sputtered with less oxygen partial pressure, the membranes were flat. However, the buckled membranes proved to be mechanically more stable, surviving higher temperatures (>220 °C), than the flat membranes (150 °C). This phenomenon was attributed to ordering of disordered vacancies, associated with lateral expansion. The material can change its dimensions reversibly and thereby respond to stress [179].

4.3. Si-based cells

Tests of μSOFCs based on Si substrates were reported in [3,248,253]. Electrodes with 500–850 nm thickness [253] were either sputtered through masks with porous microstructure, or, when sputtering was done that resulted in a dense microstructure, pores were etched in the electrodes after deposition. Ni was used for the anode, silver for the cathode. The electrolyte was dense sputtered YSZ with a thickness of 2.5 μm. A free-standing membrane of this tri-layer was obtained by wet etching a Si wafer with SiN masking and SiN etch stop which was subsequently removed by dry etching. A power output of 3.8 mW cm^{-2} was obtained at 316 °C and the OCV was 0.8 V. The geometries of the free-standing membranes were not given and for dense electrodes no output could be measured [253]. At 600 °C a maximum power of 145 mW cm^{-2} and an OCV of 1.0 V was reported [248]. In this case the micromachining was modified to obtain membranes of 5 μm size, with the thickness of each layer between 500 nm and 10 μm.

Another very recent publication [3] shows very high power densities of 200 and 400 mW cm^{-2} at 350 and 400 °C, respectively. A very thin electrolyte consisting of 50 nm YSZ and 50 nm CGO was sputtered on a SiN/Si substrate, wet and dry etching was done to structure the substrate and afterwards porous Pt (80 nm) was sputtered for use as an anode and cathode. With only YSZ as electrolyte the power output was less, 130, 85 and 60 mW cm^{-2} at 350 °C for 50, 100 and 150 nm electrolyte thickness. This would indicate a strong relation between electrolyte thickness and cell performance although the authors report the ASR of the electrodes to be one order of magnitude larger than the contribution of the electrolyte. Further studies are necessary to fully understand the behavior of μSOFCs.

The area of the free-standing membrane can be enlarged by mechanically supporting the membrane with a Ni-grid, which can also be used as a current collector [254].

4.4. Ni-based cells

Ni was also used as substrate for a μSOFC. Kang et al. [255] used sputtered Pt as an anode catalyst on a nano-porous Ni support. On top, a YSZ electrolyte 200 nm thick was sputtered, followed by porous sputtered Pt as a cathode layer. The maximum power density obtained at 400 °C was 7 mW cm^{-2}. Chen et al. used Ni foils as substrates [43]. PLD was used to deposit YSZ films 2 μm thick on Ni foils 6 μm thick. The Ni foil was then patterned with pores of about 70 μm. Afterwards a porous LSC cathode layer with 6 μm thickness was deposited also using PLD and, to increase the triple phase boundary at the anode side, a 6-μm-thick NiO-YSZ anode was added to the Ni foil. A power output of 110 mW cm^{-2} at 570 °C was achieved and an OCV of 0.8 V. The total thickness of the cell was only about 20 μm and thus one order of magnitude thinner than thin film μSOFCs based on silicon substrates.

4.5. Glass-ceramic based cells

Glass-ceramics capable of being photo-structured can also be used as micromachinable substrates for μSOFCs [9,262]. The advantages are a TEC close to that of SOFC materials and the possibility of rapid wet etching during fabrication of the free standing membrane.

5. Summary and conclusion

Many different techniques are available for thin film deposition of SOFC materials. Each method has its own advantages and drawbacks concerning microstructure and quality of the deposited films. Process complexity, choice of material, large area coating, equipment and process costs also have to be taken into account when it comes to industrial fabrication of thin films.

Sputtering is an easy process applicable to any material, with which large surfaces can be coated. For this reason it is largely employed in the industrial production of thin films. The films have a very high quality in terms of purity and surface smooth-

ness, but controlling the films' stoichiometry and the growing of complex compounds can be difficult and require the use of multiple targets.

PLD is still a laboratory method requiring expensive equipment. With this method it is relatively easy to deposit compounds with complex composition and good control of stoichiometry from single ceramic targets. The film quality is comparable to that obtained by sputtering, but surface coverage with uniform thickness is limited to few square centimeters.

CVD derived processes have the advantage of a high deposition rate and large area coverage of good quality even on complex morphologies. It can be employed for mass production. The precise control of the chemical processes involved can make this method somehow difficult and residuals from the precursors can be present in the final product reducing the purity of the film. A high temperature of typically 600–900 °C [256] of deposition is needed for the reaction to take place and corrosive gases are often present depending on the material to be deposited and the precursors chosen.

In contrast to PVD techniques, liquid precursor based thin film deposition generally results in isotropic microstructures and porous films are also easier to obtained. The great number of different deposition techniques using liquid precursors and the huge variety of the precursor chemistry, allows for many different applications of these techniques. On the other hand, this variety makes it difficult to find parameters in the literature, for a given deposition task, since most likely the setup, the atomization method, or the precursor chemistry differs.

For thin film electrolytes it was found that the change of the electrical properties with the microstructure (i.e. ratio of grain:grain boundary area) and microstrain requires detailed studies to understand these phenomena. Although nanocrystalline thin film electrolytes show lower conductivity than microcrystalline samples, the resistance of thin film electrolytes is expected to be lower due to geometrical reasons. However, a less-than-linear relationship between electrolyte thickness and electrolyte resistance in an SOFC has to be taken into account.

Only a few experimental and simulation studies on thin film anodes have been carried out by now. All relevant studies focus on Ni line pattern electrodes. Most of the results are rather preliminary by now due to the complexity of the system as well as the missing of basic kinetic data on the system. However, several studies are continued so that more detailed results are expected in the near future. Even less work has been carried out on porous thin film anodes so far but with increasing interest in μSOFC, more studies in this field can be expected.

Similar to anodes, the research on thin film cathodes has helped to better understand the cathode reaction. However, new issues have also appeared during these investigations. Only a few studies were carried out on porous thin film cathodes, but again, the emergence of μSOFCs will stimulate more research in this field.

When it comes to entire cells, calculations of geometrical constraints of μSOFCs are useful particularly for evaluating their electrochemical performance. From these results it is clear that a reduction of electrolyte thickness below 500 nm is not meaningful (depending on the electrode grain size) and that the electrodes limit the performance of μSOFCs. Geometrical restrictions for single-chamber μSOFCs are severe. Calculations of the mechanical stability seem to be only of limited use, since the complex behavior of the material is not well represented by those calculations. Modeling of the expected heat losses indicates that thermal insulation is an important issue in fabrication of μSOFCs. Stability tests of free-standing electrolytes and complete μSOFCs suggest that rather small membranes of about 100 μm feature size are feasible. Cells with high power output at very low temperatures (350–400 °C) were fabricated and showed a strong influence of the electrolyte thickness on the cell performance. This was not expected from modeling work and needs further work to understand μSOFCs, especially since the electrodes were identified to govern the cell performance. The use of Ni foils instead of Si as the substrate allows a further reduction of cell thickness; glass-ceramic substrates have better thermal properties than Si.

More work will be carried out on μSOFCs to analyze the complex mechanical and electrochemical behavior of these nano- and micro-sized materials in SOFCs. The next challenges in terms of μSOFCs production will be fabrication and contacting of an array of μSOFCs, since it also requires strong process control to obtain a reasonable yield. Stacking and housing, start-up operation and thermally self-sustained operation of a portable device are also big challenges for micro-fabrication and process engineering. However, the research carried out so far already proves that the concept of a μSOFC is realizable and that high power density at low temperatures can be expected. Hence, new applications of SOFCs are foreseen for the future.

Acknowledgment

Financial support from Swiss Bundesamt für Energie under the project OneBat – Start and Kommission für Technik und Innovation OneBat Discovery Project and The financial support by the European Union, IP-project REAL-SOFC (SES6-CT-2003-502612), are gratefully acknowledged.

References

[1] S.C. Singhal, K. Kendall, High Temperature Solid Oxide Fuel Cells: Fundamentals, Design and Applications, Elsevier Advanced Technology, Oxford, UK, 2003.
[2] Z.P. Shao, S.M. Haile, Nature 431 (2004) 170–173.
[3] H. Huang, M. Nakamura, P. Su, R. Fasching, Y. Saito, F.B. Prinz, J. Electrochem. Soc. 154 (2007) B20–B24.
[4] T. Hibino, S.Q. Wang, S. Kakimoto, M. Sano, Electrochem. Solid State Lett. 2 (1999) 317–319.
[5] T. Hibino, H. Iwahara, Chem. Lett. (1993) 1131–1134.
[6] K. Asano, T. Hibino, H. Iwahara, J. Electrochem. Soc. 142 (1995) 3241–3245.
[7] T. Hibino, A. Hashimoto, M. Yano, M. Suzuki, S. Yoshida, M. Sano, J. Electrochem. Soc. 149 (2002) A133–A136.
[8] M. Yano, A. Tomita, M. Sano, T. Hibino, Solid State Ionics 177 (2007) 3351–3359.
[9] A. Bieberle-Hütter, D. Beckel, U.P. Muecke, J.L.M. Rupp, A. Infortuna, L.J. Gauckler, Mstnews 04/05 (2005) 12–15.
[10] D. Nikbin, Fuel Cell Rev. (2006) 21–24.
[11] M. Ohring, Materials Science of Thin Films, second ed., Academic Press, 2002, pp. 57–94.

[12] L.R. Pederson, P. Singh, X.D. Zhou, Vacuum 80 (2006) 1066–1083.
[13] J. Will, A. Mitterdorfer, C. Kleinlogel, D. Perednis, L.J. Gauckler, Solid State Ionics 131 (2000) 79–96.
[14] M. Messier, A.P. Giri, R.A. Roy, J. Vac. Sci. Technol., A 2 (1983) 500–503.
[15] K.H. Guenther, in: M.R. Jacobson (Ed.), Proceedings of Modeling of Optical Thin Films II, SPIE, San Diego, CA, USA, 1990, pp. 2–12.
[16] R.A. Baragiola, Philos. Trans. R. Soc. Lond. Ser. A-Math. Phys. Eng. Sci. 362 (2004) 29–53.
[17] P.J. Kelly, R.D. Arnell, Vacuum 56 (2000) 159–172.
[18] J. Musil, P. Baroch, J. Vlcek, K.H. Nam, J.G. Han, Thin Solid Films 475 (2005) 208–218.
[19] I. Safi, Surf. Coat. Technol. 127 (2000) 203–219.
[20] E.S. Thiele, L.S. Wang, T.O. Mason, S.A. Barnett, J. Vac. Sci. Technol., A 9 (1991) 3054–3060.
[21] J.L. Hertz, H.L. Tuller, J. Electroceram. 13 (2004) 663–668.
[22] E. Gourba, A. Ringuede, M. Cassir, A. Billard, J. Paiviasaari, J. Niinisto, M. Putkonen, L. Niinisto, Ionics 9 (2003) 15–20.
[23] E. Gourba, P. Briois, A. Ringuede, M. Cassir, A. Billard, J. Solid State Electrochem. 8 (2004) 633–637.
[24] T. Tsai, S.A. Barnett, J. Vac. Sci. Technol., A 13 (1995) 1073–1077.
[25] A. Nagata, H. Okayama, Vacuum 66 (2002) 523–529.
[26] A. Bieberle-Hütter, H.L. Tuller, J. Electroceram. 16 (2006) 151–157.
[27] L.S. Wang, S.A. Barnett, Solid State Ionics 61 (1993) 273–276.
[28] J.A. Greer, M.D. Tabat, J. Vac. Sci. Technol., A 13 (1995) 1175–1181.
[29] J.A. Greer, M.D. Tabat, C. Lu, Nucl. Instrum. Methods Phys. Res. Sect. B-Beam Interact. Mater. Atoms 121 (1997) 357–362.
[30] M.N.R. Ashfold, F. Claeyssens, G.M. Fuge, S.J. Henley, Chem. Soc. Rev. 33 (2004) 23–31.
[31] J. Dieleman, E. Vanderiet, J.C.S. Kools, Jpn. J. Appl. Phys. 1 (31) (1992) 1964–1971.
[32] N. Imanishi, T. Matsumura, Y. Sumiya, K. Yoshimura, A. Hirano, Y. Takeda, D. Mori, R. Kanno, Solid State Ionics 174 (2004) 245–252.
[33] X. Chen, N.J. Wu, D.L. Ritums, A. Ignatiev, Thin Solid Films 342 (1999) 61–66.
[34] M. Prestat, A. Infortuna, S. Korrodi, S. Rey-Mermet, P. Muralt, L.J. Gauckler, J. Electroceram. 118 (2007) 111–120.
[35] L.G. Coccia, G.C. Tyrrell, J.A. Kilner, D. Waller, R.J. Chater, I.W. Boyd, Appl. Surf. Sci. 96–98 (1996) 795–801.
[36] J.L.M. Rupp, A. Infortuna, L.J. Gauckler, Acta Mater. 54 (2006) 1721–1730.
[37] J.L.M. Rupp, A. Infortuna, L.J. Gauckler, J. Am. Ceram. Soc., in press.
[38] B. Hobein, F. Tietz, D. Stover, E.W. Kreutz, J. Power Sources 105 (2002) 239–242.
[39] F. Mitsugi, S. Kanazawa, Y. Maeda, S. Suita, T. Ohkubo, Y. Nomoto, Y. Takita, Proceedings of 39th IAS Annual Meeting Industry Applications Conference, Seattle, WA, USA, 2004, pp. 1954–1958.
[40] T. Mathews, J.R. Sellar, B.C. Muddle, P. Manoravi, Chem. Mater. 12 (2000) 917–922.
[41] P. Manoravi, N. Sivakumar, M. Joseph, T. Mathews, Ionics 10 (2004) 32–38.
[42] J.W. Yan, H. Matsumoto, T. Akbay, T. Yamada, T. Ishihara, J. Power Sources 157 (2006) 714–719.
[43] X. Chen, N.J. Wu, L. Smith, A. Ignatiev, Appl. Phys. Lett. 84 (2004) 2700–2702.
[44] A. Infortuna, A. Harvey, L.J. Gauckler, submitted to Adv. Func. Mater.
[45] G.Y. Meng, H.Z. Song, Q. Dong, D.K. Peng, Solid State Ionics 175 (2004) 29–34.
[46] K.L. Choy, Prog. Mater. Sci. 48 (2003) 57–170.
[47] B.D. Fahlman, Curr. Org. Chem. 10 (2006) 1021–1033.
[48] G. Garcia, J. Caro, J. Santiso, J.A. Pardo, A. Figueras, A. Abrutis, Chem. Vapor. Depos. 9 (2003) 279–284.
[49] Y. Liu, W. Rauch, S.W. Zha, M.L. Liu, Solid State Ionics 166 (2004) 261–268.
[50] L. Niinisto, M. Ritala, M. Leskela, Mater. Sci. Eng., B 41 (1996) 23–29.
[51] C. Bernay, A. Ringuede, P. Colomban, D. Lincot, M. Cassir, J. Phys. Chem. Solids 64 (2003) 1761–1770.
[52] M. Cassir, F. Goubin, C. Bernay, P. Vernoux, D. Lincot, Appl. Surf. Sci. 193 (2002) 120–128.
[53] J.C. Viguie, J. Spitz, J. Electrochem. Soc. 122 (1975) 585–588.
[54] G.L. Messing, S.C. Zhang, G.V. Jayanthi, J. Am. Ceram. Soc. 76 (1993) 2707–2726.
[55] K. Wegner, S.E. Pratsinis, Powder Technol. 150 (2005) 117–122.
[56] P.S. Patil, Mater. Chem. Phys. 59 (1999) 185–198.
[57] B.R. Pamplin, Prog. Cryst. Growth Charact. Mater. 1 (1979) 395–403.
[58] M.S. Tomar, F.J. Garcia, Prog. Cryst. Growth Charact. Mater. 4 (1981) 221–248.
[59] S.C. Tjong, H. Chen, Mater. Sci. Eng., R 45 (2004) 1–88.
[60] J.B. Mooney, S.B. Radding, Annu. Rev. Mater. Sci. 12 (1982) 81–101.
[61] D.S. Albin, S.H. Risbud, Adv. Ceram. Mater. 2 (1987) 243–252.
[62] K.L. Chopra, S. Major, D.K. Pandya, Thin Solid Films 102 (1983) 1–46.
[63] K.L. Chopra, R.C. Kainthla, D.K. Pandya, A.P. Thakoor, Phys. Thin Films 12 (1982) 167–235.
[64] P. Bohac, L.J. Gauckler, in: H.L. Tuller (Ed.), Oxygen Ion and Mixed Conductors and Their Technological Applications, Kluwer Academic Press, Netherlands, 2000, pp. 271–294.
[65] D. Perednis, Thin Film Deposition by Spray Pyrolysis and the Application in Solid Oxide Fuel Cells, Ph.D. thesis no. 15190 ETH Zurich, Zurich, Switzerland, 2003.
[66] L.C. de Jonghe, C.P. Jacobson, S.J. Visco, Annu. Rev. Mater. Res. 33 (2003) 169–182.
[67] C.H. Chen, M.H.J. Emond, E.M. Kelder, B. Meester, J. Schoonman, J. Aerosol Sci. 30 (1999) 959–967.
[68] I. Taniguchi, R.C. van Landschoot, J. Schoonman, Solid State Ionics 156 (2003) 1–13.
[69] C.Y. Fu, C.L. Chang, C.S. Hsu, B.H. Hwang, Mater. Chem. Phys. 91 (2005) 28–35.
[70] A. Princivalle, D. Perednis, R. Neagu, E. Djurado, Chem. Mater. 16 (2004) 3733–3739.
[71] A. Princivalle, D. Perednis, R. Neagu, E. Djurado, Chem. Mater. 17 (2005) 1220–1227.
[72] E.M. Kelder, O.C.J. Nijs, J. Schoonman, Solid State Ionics 68 (1994) 5–7.
[73] H. Nomura, S. Parekh, J.R. Selman, S. Al-Hallaj, J. Appl. Electrochem. 35 (2005) 61–67.
[74] R. Neagu, D. Perednis, A.S. Princivalle, E. Djurado, Chem. Mater. 17 (2005) 902–910.
[75] O. Wilhelm, S.E. Pratsinis, D. Perednis, L.J. Gauckler, Thin Solid Films 479 (2005) 121–129.
[76] I. Taniguchi, R.C. van Landschoot, J. Schoonman, Solid State Ionics 160 (2003) 271–279.
[77] Y. Liu, M.L. Liu, J. Am. Ceram. Soc. 87 (2004) 2139–2142.
[78] F.L. Yuan, C.H. Chen, E.M. Kelder, J. Schoonman, Solid State Ionics 109 (1998) 119–123.
[79] R. Kavitha, S.R. Hegde, V. Jayaram, Mater. Sci. Eng., A 359 (2003) 18–23.
[80] W.B. Carter, G.W. Book, T.A. Polley, D.W. Stollberg, J.M. Hampikian, Thin Solid Films 347 (1999) 25–30.
[81] S. Charojrochkul, K.L. Choy, B.C.H. Steele, J. Eur. Ceram. Soc. 24 (2004) 2515–2526.
[82] T. Setoguchi, M. Sawano, K. Eguchi, H. Arai, Solid State Ionics 40–41 (1990) 502–505.
[83] P. Bohac, L. Gauckler, Solid State Ionics 119 (1999) 317–321.
[84] D. Perednis, O. Wilhelm, S.E. Pratsinis, L.J. Gauckler, Thin Solid Films 474 (2005) 84–95.
[85] D. Perednis, M.B. Joerger, K. Honegger, L.J. Gauckler, in: H. Yokokawa, S.C. Singhal (Eds.), Proceedings of 7th International Symposium on Solid Oxide Fuel Cells (SOFC VII), Tsukuba, Japan, 2001, pp. 989–994.
[86] D. Perednis, L.J. Gauckler, Solid State Ionics 166 (2004) 229–239.
[87] J.L.M. Rupp, C. Solenthaler, P. Gasser, U.P. Muecke, L.J. Gauckler, Acta Mater. 55 (2007) 3505–3512.
[88] J.L.M. Rupp, T. Drobek, A. Rossi, L.J. Gauckler, Chem. Mater. 19 (2006) 1134–1142.
[89] D. Beckel, A. Dubach, A.R. Studart, L.J. Gauckler, J. Electroceram. 16 (2006) 221–228.
[90] D. Beckel, U.P. Muecke, T. Gyger, G. Florey, A. Infortuna, L.J. Gauckler, Solid State Ionics 178 (2007) 407–415.

[91] D. Beckel, D. Briand, A.R. Studart, N.F. De Rooij, L.J. Gauckler, Adv. Mater. 18 (2006) 3105–3108.
[92] U.P. Muecke, N. Luechinger, L.J. Gauckler, Thin Solid Films, submitted for publication.
[93] U.P. Muecke, G.L. Messing, L.J. Gauckler, Thin Solid Films, submitted for publication.
[94] E.S. Putna, J. Stubenrauch, J.M. Vohs, R.J. Gorte, Langmuir 11 (1995) 4832–4837.
[95] P. Charpentier, P. Fragnaud, D.M. Schleich, C. Lunot, E. Gehain, Ionics 3 (1997) 155–160.
[96] P. Charpentier, P. Fragnaud, D.M. Schleich, Y. Denos, E. Gehain, Ionics 4 (1998) 118–123.
[97] P. Charpentier, P. Fragnaud, D.M. Schleich, E. Gehain, Solid State Ionics 135 (2000) 373–380.
[98] N.X.P. Vo, S.P. Yoon, S.W. Nam, J. Han, T.H. Lim, S.A. Hong, On the Convergence of Bio-Information-, Environmental-, Energy-, Space- and Nano-Technologies, Pts 1 and 2, 2005, pp. 455-461.
[99] Y. Matsuzaki, M. Hishinuma, I. Yasuda, Thin Solid Films 340 (1999) 72–76.
[100] A. Furusaki, H. Konno, R. Furuichi, J. Mater. Sci. 30 (1995) 2829–2834.
[101] S. Wang, W. Wang, Q. Liu, M. Zhang, Y. Qian, Solid State Ionics 133 (2000) 211–215.
[102] M.A. Priestnall, B.C.H. Steele, in: S.C. Singhal (Ed.), Proceedings of 1st International Symposium on Solid Oxide Fuel Cells (SOFC I), 1989, pp. 157–167.
[103] Z.Y. Peng, M.L. Liu, J. Am. Ceram. Soc. 84 (2001) 283–288.
[104] L. Jia, Z. Lu, X.Q. Huang, Z.G. Liu, K.F. Chen, X.Q. Sha, G.Q. Li, W.H. Su, J. Alloys Compd. 424 (2006) 299–303.
[105] M. Matsuda, T. Hosomi, K. Murata, T. Fukui, M. Miyakea, Electrochem. Solid State Lett. 8 (2005) A8–A11.
[106] P.Y. Chu, R.C. Buchanan, J. Mater. Res. 6 (1991) 1736–1743.
[107] K. Hayashi, M. Hosokawa, T. Yoshida, Y. Ohya, Y. Takahashi, O. Yamamoto, H. Minoura, Mater. Sci. Eng., B 49 (1997) 239–242.
[108] J.V. Mantese, A.L. Micheli, A.B. Catalan, N.W. Schubring, Appl. Phys. Lett. 64 (1994) 3509–3511.
[109] D.T. Morelli, A.M. Mance, J.V. Mantese, A.L. Micheli, J. Appl. Phys. 79 (1996) 373–375.
[110] C.J. Brinker, G.C. Frye, A.J. Hurd, C.S. Ashley, Thin Solid Films 201 (1991) 97–108.
[111] C.J. Brinker, A.J. Hurd, P.R. Schunk, G.C. Frye, C.S. Ashley, J. Non-Cryst. Solids 147 (1992) 424–436.
[112] B. Dunn, G.C. Farrington, B. Katz, Solid State Ionics 70/71 (1994) 3–10.
[113] C.C. Chen, M.M. Nasrallah, H.U. Anderson, J. Electrochem. Soc. 140 (1993) 3555–3560.
[114] R.M. Smith, X.D. Zhou, W. Huebner, H.U. Anderson, J. Mater. Res. 19 (2004) 2708–2713.
[115] P. Lenormand, S. Castillo, J.-R. Gonzalez, C. Laberty-Robert, F. Ansart, Solid State Sci. 7 (2005) 159–163.
[116] S.-G. Kim, S.P. Yoon, S.W. Nam, S.-H. Hyun, S.-A. Hong, J. Power Sources 110 (2002) 222–228.
[117] S.-G. Kim, S.W. Nam, S.-P. Yoon, S.-H. Hyun, J. Han, T.-H. Lim, S.-A. Hong, J. Mater. Sci. 39 (2004) 2683–2688.
[118] W.S. Jang, S.H. Hyun, S.G. Kim, J. Mater. Sci. 37 (2002) 2535–2541.
[119] K. Mehta, R. Xu, A.V. Virkar, J. Sol–Gel Sci. Technol. 11 (1998) 203–207.
[120] P. Peshev, V. Slavova, Mater. Res. Bull. 27 (1992) 1269–1275.
[121] X. Changrong, C. Huaqiang, W. Hong, Y. pinghua, M. Guangyao, P. Dingkun, J. Membr. Sci. 162 (1999) 181–188.
[122] H.J. Hwang, J. Moon, M. Awano, K. Maeda, J. Am. Ceram. Soc. 83 (2000) 2852–2854.
[123] H.J. Hwang, A. Towata, M. Awano, J. Am. Ceram. Soc. 84 (2001) 2323–2327.
[124] H.J. Hwang, A. Towata, M. Awano, K. Maeda, Scripta Mater. 44 (2001) 2173–2177.
[125] B.P. Gorman, H.U. Anderson, J. Am. Ceram. Soc. 84 (2001) 890–892.
[126] J.H. Dong, M.Z. Hu, E.A. Payzant, T.R. Armstrong, P.F. Becher, J. Nanosci. Nanotechnol. 2 (2002) 161–169.
[127] C.C. Chen, M.M. Nasrallah, H.U. Anderson, Solid State Ionics 70/71 (1994) 101–108.
[128] T. Brezesinski, M. Antonietti, M. Groenewolt, N. Pinna, B. Smarsly, New J. Chem. 29 (2005) 237–242.
[129] S.C. Wang, H.Z. Hsu, W.J. Wei, Key Eng. Mater. 247 (2003) 393–396.
[130] M. Gaudon, C. Laberty-Robert, F. Ansart, P. Stevens, A. Rousset, Solid State Sci. 4 (2002) 125–133.
[131] M. Gaudon, C. Laberty-Robert, E. Ansart, P. Stevens, A. Rousset, Solid State Sci. 5 (2003) 1377–1383.
[132] M.P. Pechini, Method of Preparing Lead and Alkaline Earth Titanates and Niobates and Coatings Method Using the Same to Form a Capacitor, Patent US 3,330,697 (1967).
[133] I. Moriguchi, H. Maeda, Y. Teraoka, S. Kagawa, J. Am. Chem. Soc. 117 (1995) 1139–1140.
[134] I. Moriguchi, H. Maeda, Y. Teraoka, S. Kagawa, Chem. Mater. 9 (1997) 1050–1057.
[135] I. Moriguchi, Y. Tsujigo, Y. Teraoka, S. Kagawa, Adv. Mater. 11 (1999) 997–1000.
[136] I. Moriguchi, Y. Tsujigo, Y. Teraoka, S. Kagawa, J. Sol–Gel Sci. Technol. 19 (2000) 227–230.
[137] I. Moriguchi, Y. Tsujigo, Y. Teraoka, S. Kagawa, J. Phys. Chem. B 104 (2000) 8101–8107.
[138] P. Jasinski, V. Petrovsky, T. Suzuki, T. Petrovsky, H.U. Anderson, J. Electrochem. Soc. 152 (2005) A454–A458.
[139] V. Petrovsky, T. Suzuki, P. Jasinski, T. Petrovsky, H.U. Anderson, Electrochem. Solid State Lett. 7 (2004) A138–A139.
[140] S.P. Yoon, J. Han, S.W. Nam, T.-H. Lim, I.-H. Oh, S.-A. Hong, Y.-S. Yoo, H.C. Lim, J. Power Sources 106 (2002) 160–166.
[141] Y.Y. Huang, K. Ahn, J.M. Vohs, R.J. Gorte, J. Electrochem. Soc. 151 (2004) A1592–A1597.
[142] A.Q. Pham, T.H. Lee, R.S. Glass, in: S.C. Singhal (Ed.), Proceedings of 6th International Conference on Solid Oxide Fuel Cells (SOFC VI), Honolulu, HI, USA, 1999, pp. 172–178.
[143] B.W. Chung, A.Q. Pham, J.J. Haslam, R.S. Glass, J. Electrochem. Soc. 149 (2002) A325–A330.
[144] Y. Du, N.M. Sammes, J. Power Sources 136 (2004) 66–71.
[145] S.D. Kim, S.H. Hyun, J. Moon, J.-H. Kim, R.H. Song, J. Power Sources 139 (2005) 67–72.
[146] Y. Zhang, J. Gao, G. Meng, X. Liu, J. Appl. Electrochem. 34 (2004) 637–641.
[147] S. de Souza, S.J. Visco, L.C. DeJonghe, Solid State Ionics 98 (1997) 57–61.
[148] S. de Souza, S.J. Visco, L.C. DeJonghe, J. Electrochem. Soc. 144 (1997) L35–L37.
[149] C.H. Wang, W.L. Worrell, S. Park, J.M. Vohs, R.J. Gorte, J. Electrochem. Soc. 148 (2001) A864–A868.
[150] Q. Zhu, B. Fan, Solid State Ionics 176 (2005) 889–894.
[151] Y. Zhang, J. Gao, D. Peng, M. Guangyao, X. Liu, Ceram. Int 30 (2004) 1049–1053.
[152] P. Knauth, H.L. Tuller, Solid State Ionics 136 (2000) 1215–1224.
[153] Y.M. Chiang, E.B. Lavik, I. Kosacki, H.L. Tuller, J.Y. Ying, Appl. Phys. Lett. 69 (1996) 185–187.
[154] J. Maier, Z. Phys. Chem. 217 (2003) 415–436.
[155] J. Maier, J. Eur. Ceram. Soc. 24 (2004) 1251–1257.
[156] A. Tschope, E. Sommer, R. Birringer, Solid State Ionics 139 (2001) 255–265.
[157] I. Kosacki, T. Suzuki, H.U. Anderson, P. Colomban, Solid State Ionics 149 (2002) 99–105.
[158] A. Michels, C.E. Krill, H. Ehrhardt, R. Birringer, D.T. Wu, Acta Mater. 47 (1999) 2143–2152.
[159] H. Natter, M. Schmelzer, M.S. Loffler, C.E. Krill, A. Fitch, R. Hempelmann, J. Phys. Chem. B 104 (2000) 2467–2476.
[160] E. Jud, C.B. Huwiler, L.J. Gauckler, J. Am. Ceram. Soc. 88 (2005) 3013–3019.
[161] F. Liu, R. Kirchheim, J. Cryst. Growth 264 (2004) 385–391.
[162] H. Gleiter, Prog. Mater. Sci. 33 (1989) 223–315.
[163] A. Atkinson, T.M.G.M. Ramos, Solid State Ionics 129 (2000) 259–269.
[164] B.C.H. Steele, J. Power Sources 49 (1994) 1–14.
[165] S.J. Skinner, J.A. Kilner, Mater. Today 6 (2003) 30–37.
[166] N.Q. Minh, J. Am. Ceram. Soc. 76 (1993) 563–588.

[167] L.J. Gauckler, D. Beckel, B.E. Buergler, E. Jud, U.P. Mücke, M. Prestat, J.L.M. Rupp, J. Richter, Chimia 58 (2004) 837–850.
[168] S.M. Haile, Acta Mater. 51 (2003) 5981–6000.
[169] B.C.H. Steele, Curr. Opin. Solid State Mater. Sci. 1 (1996) 684–691.
[170] V.V. Kharton, F.M.B. Marques, A. Atkinson, Solid State Ionics 174 (2004) 135–149.
[171] R.M. Ormerod, Chem. Soc. Rev. 32 (2002) 17–28.
[172] C. Kleinlogel, L.J. Gauckler, Solid State Ionics 135 (2000) 567–573.
[173] M. Gödickemeier, K. Sasaki, L.J. Gauckler, J. Electrochem. Soc. 144 (1997) 1635–1645.
[174] D. Schneider, M. Godickemeier, L.J. Gauckler, J. Electroceram. 1 (1997) 165–172.
[175] I. Riess, M. Godickemeier, L.J. Gauckler, Solid State Ionics 90 (1996) 91–104.
[176] I. Riess, Solid State Ionics 157 (2003) 1–17.
[177] Y. Mizutani, M. Tamura, M. Kawai, O. Yamamoto, Solid State Ionics 72 (1994) 271–275.
[178] S.Y. Chun, N. Mizutani, Appl. Surf. Sci. 171 (2001) 82–88.
[179] M. Greenberg, E. Wachtel, I. Lubomirsky, J. Fleig, J. Maier, Adv. Funct. Mater. 16 (2006) 48–52.
[180] J.L.M. Rupp, L.J. Gauckler, Solid State Ionics 177 (2006) 2513–2518.
[181] A. Atkinson, Solid State Ionics 95 (1997) 249–258.
[182] J. Fleig, H.L. Tuller, J. Maier, Solid State Ionics 174 (2004) 261–270.
[183] T. Kudo, Y. Obayashi, J. Electrochem. Soc. 123 (1976) 415.
[184] M. Mogensen, N.M. Sammes, G.A. Tompsett, Solid State Ionics 129 (2000) 63–94.
[185] T. Suzuki, I. Kosacki, H.U. Anderson, Solid State Ionics 151 (2002) 111–121.
[186] A.O. Stoermer, J.L.M. Rupp, L.J. Gauckler, Solid State Ionics 177 (2006) 2075–2079.
[187] M. Gödickemeier, L.J. Gauckler, J. Electrochem. Soc. 145 (1998) 414–421.
[188] T. Mathews, P. Manoravi, M.P. Antony, J.R. Sellar, B.C. Muddle, Solid State Ionics 135 (2000) 397–402.
[189] T. Takeyama, N. Takahashi, T. Nakamura, S. Itoh, Surf. Coat. Technol. 16/17 (2006) 4797–4801.
[190] T. Takeyama, N. Takahashi, T. Nakamura, S. Itoh, J. Cryst. Growth 275 (2005) 460–466.
[191] T. Takeyama, N. Takahashi, T. Nakamura, S. Itoh, J. Cryst. Growth 277 (2005) 485–489.
[192] P. Shuk, H.-D. Wiemhofer, U. Guth, W. Gopel, M. Greenblatt, Solid State Ionics 89 (1996) 179–196.
[193] N.M. Sammes, G.A. Tompsett, H. Nafe, F. Aldinger, J. Eur. Ceram. Soc. 19 (1999) 1801–1826.
[194] R.J. Aaberg, R. Tunold, M. Mogensen, R.W. Berg, R. Odegrd, J. Electrochem. Soc. 145 (1998) 2244–2252.
[195] R.J. Aaberg, R. Tunold, R. Odegard, Solid State Ionics 136/137 (2000) 707–712.
[196] D. Kek, M. Mogensen, S. Pejovnik, J. Electrochem. Soc. 148 (2001) A878–A886.
[197] K. Vels Jensen, S. Primdahl, I. Chorkendorff, M. Mogensen, Solid State Ionics 144 (2001) 197–209.
[198] S.P. Jiang, S.P.S. Badwal, J. Electrochem. Soc. 144 (1997) 3777–3784.
[199] J. Mizusaki, H. Tagawa, T. Saito, T. Yamamura, K. Kamitani, K. Hirano, S. Ehara, T. Takagi, T. Hikita, M. Ippommatsu, S. Nakagawa, K. Hashimoto, Solid State Ionics 70/71 (1994) 52–58.
[200] B. de Boer, Hydrogen oxidation at porous nickel and nickel/yittria stabilized zirconia cermet electrodes, Ph.D. thesis, University of Twente, Twente, Netherlands, 1998.
[201] A. Bieberle, L.P. Meier, L.J. Gauckler, J. Electrochem. Soc. 148 (2001) A646–A656.
[202] A.M. Sukeshini, B. Habibzadeh, in: S.C. Singhal, J. Mizusaki (Eds.), Proceedings of 9th International Symposium on Solid Oxide Fuel Cells (SOFC-IX), Quebec City, Canada, 2005.
[203] A. Ehn, J.J. Hogh, in: S. Linderoth, A. Smith, N. Bonanos, A. Hagen, L. Mikkelsen, K. Kammer, D. Lybye, P.V. Hendriksen, F.W. Poulsen, M. Mogensen, W.G. Wang (Eds.), Proceedings of 26th Risoe International Symposium on Materials Science: High-temperature Electrochemistry, Roskilde, Denmark, 2005.
[204] A. Bieberle, L.J. Gauckler, Solid State Ionics 146 (2002) 23–41.
[205] W.G. Bessler, Solid State Ionics 176 (2005) 997–1011.
[206] W.G. Bessler, S. Gewies, in: S.C. Singhal, J. Mizusaki (Eds.), Proceedings of 9th International Symposium on Solid Oxide Fuel Cells (SOFC IX), Quebec City, Canada, 2005.
[207] W.G. Bessler, J. Electrochem. Soc. 153 (2006) A1492–A1504.
[208] D.G. Goodwin, in: S.C. Singhal, J. Mizusaki (Eds.), Proceedings of 9th International Symposium on Solid Oxide Fuel Cells (SOFC-IX), Quebec City, Canada, 2005.
[209] R.E. Williford, L.A. Chick, Surf. Sci. 547 (2003) 421–437.
[210] G.J. la O, J. Hertz, H. Tuller, Y. Shao-Horn, J. Electroceram. 13 (2004) 691–695.
[211] S.B. Adler, Chem. Rev. 104 (2004) 4791–4843.
[212] S. Wang, M. Katsuki, M. Dokiya, T. Hashimoto, Solid State Ionics 159 (2003) 71–78.
[213] H.U. Anderson, Solid State Ionics 52 (1992) 33–41.
[214] J.W. Stevenson, T.R. Armstrong, R.D. Carneim, L.R. Pederson, W.J. Weber, J. Electrochem. Soc. 143 (1996) 2722–2729.
[215] T. Horita, K. Yamaji, M. Ishikawa, N. Sakai, H. Yokokawa, T. Kawada, T. Kato, J. Electrochem. Soc. 145 (1998) 3196–3202.
[216] T. Horita, K. Yamaji, N. Sakai, H. Yokokawa, T. Kawada, T. Kato, Solid State Ionics 127 (2000) 55–65.
[217] T. Horita, K. Yamaji, N. Sakai, H. Yokokawa, T. Kato, J. Electrochem. Soc. 148 (2001) J25–J30.
[218] V. Brichzin, J. Fleig, H.-U. Habermeier, J. Maier, Electrochem. Solid-State Lett. 3 (2000) 403–406.
[219] V. Brichzin, J. Fleig, H.-U. Habermeier, G. Cristiani, J. Maier, Solid State Ionics 152–153 (2002) 499–507.
[220] R.A. de Souza, J.A. Kilner, J.F. Walker, Mater. Lett. 43 (2000) 43–52.
[221] F.S. Baumann, J. Fleig, J. Maier, in: M. Mogensen (Ed.), Proceedings of 6th European Solid Oxide Forum, Lucerne, Switzerland, 2004, pp. 1241–1252.
[222] E. Koep, C. Compson, M. Liu, Z. Zhou, Solid State Ionics 176 (2005) 1–8.
[223] B. Yildiz, G.J. La O, Y. Shao-Horn, J. Electrochem. Soc., submitted for publication.
[224] M. Prestat, Oxygen reduction in solid oxide fuel cells at intermediate temperatures: state-space modelling and experimental validation, Ph.D. thesis nr. 16142 ETH Zurich, Zurich, Switzerland, 2006.
[225] M. Prestat, J.-F. Koenig, L.J. Gauckler, J. Electroceram. 18 (2007) 87–101.
[226] J. Jamnik, J. Maier, J. Electrochem. Soc. 146 (1999) 4183–4188.
[227] A. Bieberle-Hütter, M. Soegaard, H.L. Tuller, Solid State Ionics 177 (2006) 1969–1975.
[228] J.D. Sirman, J.A. Lane, J.A. Kilner, in: T.A. Ramanarayanan, W.L. Worrel, T.H. L, A.C. Khandkar, M. Mogensen, W. Gopel (Eds.), Proceedings of Ionic and Mixed Conducting Ceramics III, Paris, France, 1997, pp. 57–72.
[229] B.C.H. Steele, J.-M. Bae, Solid State Ionics 106 (1998) 255–261.
[230] F.S. Baumann, J. Fleig, M. Konuma, U. Starke, H.-U. Habermeier, J. Maier, J. Electrochem. Soc. 152 (2005) A2074–A2079.
[231] S.P. Jiang, Solid State Ionics 146 (2002) 1–22.
[232] A. Esquirol, N.P. Brandon, J.A. Kilner, M. Mogensen, J. Electrochem. Soc. 151 (2004) A1847–A1855.
[233] A. Ringuede, J. Fouletier, Solid State Ionics 139 (2001) 167–177.
[234] Y.L. Yang, C.L. Chen, S.Y. Chen, C.W. Chu, A.J. Jacobson, J. Electrochem. Soc. 147 (2000) 4001–4007.
[235] A. Endo, H. Fukunaga, C. Wen, K. Yamada, Solid State Ionics 135 (2000) 353–358.
[236] T. Kawada, J. Suzuki, M. Sase, A. Kaimai, K. Yashiro, Y. Nigara, J. Mizusaki, K. Kawamura, H. Yugami, J. Electrochem. Soc. 149 (2002) E252–E259.
[237] S. Diethelm, A. Closset, J. Van Herle, K. Nisancioglu, Electrochemistry 68 (2000) 444.
[238] M.S. Islam, Solid State Ionics 154–155 (2002) 75–85.

[239] M. Cherry, M.S. Islam, C.R.A. Catlow, J. Solid State Chem. 118 (1995) 125–132.
[240] L. Gavrilova, V.A. Cherepanov, in: S.C. Singhal, M. Dokiya (Eds.), Proceedings of 6th Internationla Conference on Solid Oxide Fuel Cells (SOFC VI), Honolulu, HI, USA, 1999, pp. 404–414.
[241] M.L. Liu, D.S. Wang, J. Mater. Res. 10 (1995) 3210–3221.
[242] C. Argirusis, T. Damjanovic, G. Borchardt, Key Eng. Mater. 314 (2006) 101–106.
[243] C.S. Hsu, B.H. Hwang, J. Electrochem. Soc. 153 (2006) A1478–A1483.
[244] S.J. Ahn, J.H. Lee, J. Kim, J. Moon, Electrochem. Solid State Lett. 9 (2006) A228–A231.
[245] B.E. Buergler, M. Ochsner, S. Vuillemin, L.J. Gauckler, J. Power Sources, submitted for publication.
[246] Y. Tang, K. Stanley, Q.M.J. Wu, D. Ghosh, J.J. Zhang, J. Micromech. Microeng. 15 (2005) S185–S192.
[247] V.T. Srikar, K.T. Turner, T.Y.A. Ie, S.M. Spearing, J. Power Sources 125 (2004) 62–69.
[248] Jankowski, J.P. Hayes, R. Tim Graff, J.D. Morse, Proc. Mater. Res. Soc. Symp. 730 (2002) 93–98.
[249] Z.P. Shao, S.M. Haile, J. Ahn, P.D. Ronney, Z.L. Zhan, S.A. Barnett, Nature 435 (2005) 795–798.
[250] C.D. Baertsch, K.F. Jensen, J.L. Hertz, H.L. Tuller, S.T. Vengallatore, S.M. Spearing, M.A. Schmidt, J. Mater. Res. 19 (2004) 2604–2615.
[251] P. Bruschi, A. Diligenti, A. Nannini, M. Piotto, Thin Solid Films 346 (1999) 251–254.
[252] J.P.W. Nair, I. Lubomirsky, J. Fleig, J. Maier, Adv. Mater. 15 (2003) 2077.
[253] A.F. Jankowski, R.T. Graff, J.P. Wayes, J.D. Morse, in: S.C. Singhal, M. Dokiya (Eds.), Proceedings of 6th International on Symposium Solid Oxide Fuel Cells (SOFC VI), Honolulu, HI, USA, 1999, pp. 932–937.
[254] S. Rey-Mermet, P. Muralt, Metallic supporting grid for thin electrolyte membrane in solid oxide fuel cell, Patent PCT/EP2006/069688 (2006).
[255] S. Kang, P.C. Su, Y.I. Park, Y. Salto, F.B. Prinz, J. Electrochem. Soc. 153 (2006) A554–A559.
[256] J.R.V. Garcia, T. Goto, Sci. Technol. Adv. Mater. 4 (2003) 397–402.
[257] H.B. Wang, C.R. Xia, G.Y. Meng, D.K. Peng, Mater. Lett. 44 (2000) 23–28.
[258] I. Kosacki, C.M. Rouleau, P.F. Becher, J. Bentley, D.H. Lowndes, Solid State Ionics 176 (2005) 1319–1326.
[259] I. Kosacki, T. Suzuki, V. Petrovsky, H.U. Anderson, Solid State Ionics 136–137 (2000) 1225–1233.
[260] G. Chiodelli, L. Malavasi, V. Massarotti, P. Mustarelli, E. Quartarone, Solid State Ionics 176 (2005) 1505–1512.
[261] L. Chen, C.L. Chen, D.X. Huang, Y. Lin, X. Chen, A.J. Jacobson, Solid State Ionics 175 (2004) 103–106.
[262] U.P. Muecke, D. Beckel, A. Bieberle-Hütter, S. Graf, A. Infortuna, J.L.M. Rupp, J. Schneider, P. Mueller, A. Bernard, L.J. Gauckler, submitted to Advanced Functional Materials (2007).